MASTER'S THESIS

A Model Predictive Approach to Satellite Formation Control

Edvards Scukins
2016

Master of Science in Engineering Technology
Space Engineering

Luleå University of Technology
Department of Computer Science, Electrical and Space Engineering

LULEÅ UNIVERSITY OF TECHNOLOGY

A model predictive approach to satellite formation control

Author:
Edvards Scukins

Supervisors:
Damiano Varagnolo
Riccardo Lucchese
Leonard Felicetti

Academic year 2015/2016

Contents

Abbreviations

CW	Clohessy-Wiltshire
ECI	Earth-centered inertial
LEO	Low Earth's orbit
LQR	Linear Quadratic Regulator
LVLH	Local Vertical Local Horizontal
MPC	Model Predictive Control
RAAN	Right ascension of the ascending node
SMPC	Stochastic Model Predictive Control
ZOH	Zero-Order Hold

Nomenclature

In this work we let scalars be indicated by lower case italics. We indicate vectors using lower case bold italics and matrices with upper case italics (besides F or $\boldsymbol{F}$, that we use for indicating scalar or vector forces). We moreover make use of the symbols and constants listed in Tables 1 and 2.

Symbol	*Description*
$\lvert\cdot\rvert$	absolute value
$m_\oplus$	mass of Earth
G	gravitational constant
μ	gravitational parameter for the Earth given by the product $m_\oplus G$
F_g	gravitational force
F_c	centripetal force (in general)
e	eccentricity (in general)
ω	periapsis (in general)
Ω	right ascension of the ascending node
s_0	debris satellite
a_0	radius of the debris' circular orbit
n_0	debris' angular velocity
$\mathcal{E}$	Earth-centered inertial (ECI) frame (assumed stationary w.r.t. the satellites)
$\widehat{\boldsymbol{I}}$	coordinate of $\mathcal{E}$ directed from the ECI center along the vernal equinox
$\widehat{\boldsymbol{K}}$	coordinate of $\mathcal{E}$ normal to the fundamental plane and positive in the direction of the geographic north pole
$\widehat{\boldsymbol{J}}$	coordinate of $\mathcal{E}$ completing $\widehat{\boldsymbol{I}}$ and $\widehat{\boldsymbol{K}}$ so that they jointly form a basis for $\mathbb{R}^3$
$\boldsymbol{r}_i^{\mathcal{E}}$	position vector of the i-th satellite in the ECI frame
$\dot{\boldsymbol{r}}_i^{\mathcal{E}}$	velocity vector of the i-th satellite in the ECI frame
$\ddot{\boldsymbol{r}}_i^{\mathcal{E}}$	acceleration vector of the i-th satellite in the ECI frame
$x_i^{\mathcal{E}}$	$\widehat{\boldsymbol{I}}$-component of the $\boldsymbol{r}_i^{\mathcal{E}}$ vector
$y_i^{\mathcal{E}}$	$\widehat{\boldsymbol{J}}$-component of the $\boldsymbol{r}_i^{\mathcal{E}}$ vector
$z_i^{\mathcal{E}}$	$\widehat{\boldsymbol{K}}$-component of the $\boldsymbol{r}_i^{\mathcal{E}}$ vector
$\mathcal{L}$	Local Vertical Local Horizontal (LVLH) frame, positioned at the debris satellite
$\boldsymbol{\theta}$	angle of the LVLH frame w.r.t. the ECI frame
$\dot{\boldsymbol{\theta}}$	angular velocity of the LVLH frame w.r.t. the ECI frame
$\boldsymbol{\rho}_i^{\mathcal{L}}$	position vector of the i-th satellite in the LVLH frame
$\dot{\boldsymbol{\rho}}_i^{\mathcal{L}}$	velocity vector of the i-th satellite in the LVLH frame
$\ddot{\boldsymbol{\rho}}_i^{\mathcal{L}}$	acceleration vector of the i-th satellite in the LVLH frame
$x_i^{\mathcal{L}}$	x-component of the $\boldsymbol{\rho}_i^{\mathcal{L}}$ vector
$y_i^{\mathcal{L}}$	y-component of the $\boldsymbol{\rho}_i^{\mathcal{L}}$ vector
$z_i^{\mathcal{L}}$	z-component of the $\boldsymbol{\rho}_i^{\mathcal{L}}$ vector
$\mathcal{S}_i$	i-th satellite's attitude frame
m_i	mass of the i-th satellite
$\boldsymbol{F}_i^{\mathcal{E}}$	Force acting on the i-th satellite in the ECI frame
$\boldsymbol{F}_i^{\mathcal{L}}$	Force acting on the i-th satellite in the LVLH frame
u_x	x-component of $\boldsymbol{F}_i^{\mathcal{L}}$
u_y	y-component of $\boldsymbol{F}_i^{\mathcal{L}}$
u_z	z-component of $\boldsymbol{F}_i^{\mathcal{L}}$
d_x	force disturbance along the direction of u_x
d_y	force disturbance along the direction of u_y
d_z	force disturbance along the direction of u_z

Table 1: Table of the most important and recurring symbols in this thesis.

Notation	*Name*	*Value*	*Unit*
G	Gravitational constant	6.67408e-11	$[m^3kg^{-1}s^{-2}]$
M	Mass of Earth	5.97219e24	$[kg]$
μ	GM	3.9859e+14	$[m^3kg^{-1}s^{-2}]$
R	Earth's radius	6371e3	$[m]$
J_2	J_2 constant	0.00108263	–
g_0	Gravitational acceleration at the sea level	9.81	$[m/s^2]$
I_{sp}	Satellite spec of Bi-propellant	340	$[Ns/kg]$

Table 2: Table of physical constants.

Abstract

It is notoriously costly to send a large satellite full of on-board instruments to space for planetary exploration and distributed physical experiments. What if, instead, we could split one large instrument into several smaller parts, and then launch each smaller part with a smaller satellite? The problem of having to launch big satellites would be solved; moreover it would also be cheaper to manufacture and launch several small satellites that one big satellite.

But, unfortunately, there is no free lunch. Splitting a big single satellite into a swarm of small micro satellites introduces the problem of maintaining these micro satellites in a certain position with respect to each other: indeed if we want our instruments to work together, on-board instruments should maintain a certain relative distance and orientation between themselves. In other words, there is the need to achieve and maintain formations, and continuously counteract the slight differences in disturbances that will act on each satellite.

This thesis then considers this need, and proposes control algorithms that guarantee swarms of satellites to maintain a certain position in space and counteract spatial disturbances.

Once again there is no free lunch: to maintain a formation and be robust with respect to disturbances there is the need for using on-board fuel. But on-board fuel is finite: as soon as it runs out, the satellites won't be able to change their orbit anymore. Our mission is then to find a control strategy that not only guarantees the satellites to maintain a formation irrespectively of the disturbances, but also to minimize fuel usage, so to increase the life of the satellites in orbit.

For all these purposes we derive and simulate a tailored stochastic centralized Model Predictive Control (MPC) approach for keeping satellites in formation while considering reference positions, fuel cost and relative position between satellites in its formulation.

More specifically we do comparison between different control approaches and study their performances. Preliminary simulations have shown that MPC is suitable for satellite formation control and can be used to control a formation on an orbit. There are still some problems, more specifically we have a centralized controller, which is not robust with respect to failures.

Chapter 1

Introduction

A satellite is usually an artificial object that has been placed in orbit. Nowadays satellites provide us with communication on a global scale and global positioning system navigation. For weather forecast, satellites in geostationary orbit that has an approximate altitude of 36 000 km, can continuously observe almost an entire hemisphere. Other satellites, such as the Hubble space telescope, can capture images of distant galaxies without interference form Earth's atmosphere. These images helps scientists understand how the universe works. As an example, astronomers that used data from Hubble space telescope have published more than 12 800 scientific papers, thus making it one of the most productive scientific instruments ever built [14].

In a lot of cases one satellite is not enough for completing a specific task, and for many future missions we need to use fleets of satellites that fly in formation. The definition of spacecraft formation flying [1] is not universally agreed upon, but we can use the definition proposed by NASA's Goddard Space Flight Center, defining it as "the tracking or maintenance of a desired relative separation, orientation or position between or among spacecrafts".

Satellite formation flying is an interesting area as it provides with many possibilities for space missions. There are many advantages of employing several small satellites instead of big ones: this can reduce the construction cost, and if a satellite has an on-board failure, it is better that it is one that is small and part of a flock, rather than it is a big and unique one. These advantages are reflected in the increasing number of experimental applications that would benefit from this paradigm, for example the Gravity Recovery And Climate Experiment (GRACE) that measures Earth's gravitational field and that consists of two trailing satellites measuring the variation of the distance between them to detect changes in the Earth's gravitational pull [5]. An other example is the LISA pathfinder [13], where 3 satellites construct a 5 million kilometer laboratory in space to detect gravitational waves and test on-board equipment in a close to perfect zero gravity environment. Since year 1957, when the first satellite was launched, there have been many other satellites launched to orbit Earth's orbits. A life expectancy of a satellite averages around 5 years, this implies that the are lots of old parts in space ranging from small mechanical pieces to large rocket boosters. More specifically, there are around 500,000 pieces of debris orbiting Earth and our mission will be to remove some of them. This thesis focuses on controlling satellite formation using a Model Predictive Control (MPC) to remove old satellites from Low Earth's orbit (LEO). Before discussing the content of the thesis, we introduce some related literature review.

1.1 Literature review

There is an increasing interest in using satellites flying in formation. The main interest comes from the possibility of reducing the cost and addition of flexibility for space-based programs as mentioned in [3]. By replacing a big satellite with several small, hope is to reduce the complexity of big satellites. Satellite formation flying methods can benefit many future mission to do distributed observations, such as synthetic apertures for Earth mapping interferometry[3].

There is a lot of research in this area to improve the performance of satellite formation flying. [16] proposes a set of linearized equations that describe the relative motion of satellites under the effect of the J_2 geopotential disturbance. The classical way of modelling the relative motion between satellites is to use linearized Hill equations. By adding the J_2 effect inside the linearized equations of motions, we can reduce the fuel consumption due to the fact that we have a more accurate equations of relative motion. By using Hill equations, [15] tested several control approaches for leader-follower formation flying. A PD controller showed to result in an exponentially stable equilibrium for a closed loop system. As for Lyapunov theory based controller, result was an asymptotically stable controller for a closed loop system. In the same paper an integrator backstepping concept was tested as well and proved to also result in a uniformly globally asymptotically stable closed loop system. For controlling satellites, there is a need for relative distance/velocity measurement system. In [17] a fully decentralized system design was tested. In this set-up each spacecraft was equipped with its own single-frequency global positioning-system receiver and navigation computer. With a continuous exchange of raw measurements between two satellites in the formation multiple Kalman filters running concurrently on each navigation computer provide estimates of both state vector and the relative state vector of all remote satellites in the formation. This set-up supports a formation up to four spacecraft with an accuracy of 1.5 mm(position) and 5 $\mu m/s$ (velocity) over a 4-km baseline. One of the main benefits of satellite formation flying is that it allows much wider range of experiment that can be done in space. As mentioned in [18], the small satellite formation can perform measurements that surpasses measurements of a single big satellite. For example The Cluster mission [6], that consists of 4 satellites, enables scientist to build a 3D model of Earth's magnetosphere and to get a better understanding of process that is taking place inside of it. As satellites are exposed to different disturbances, such as drag force and pressure from solar wind, a counteractive adjustments need to be made. As in LISA satellite formation case [2], the closed loop was based proportional-derivative (PD) controller and used to counteract disturbances. There are several different thruster methods that can be used for maintaining a formation. One of the most efficient thrusters are the ion thrusters, but even these instruments have uncertainty. In [11] was mentioned that ion thrusters magnitude have an accuracy of 1.2 % with a maximum absolute error of 0.5 mN and misalignment from 0.5 deg to 5 deg. Thus the thrust uncertainty and misalignment can be a serious problem when setting up a minimum fuel usage system. Thus to enable many other future missions and space related scientific experiments, a fuel efficient control algorithm is needed. [9] Presents fuel/time-optimal control algorithm for co-ordination and control architecture that was designed for fleet of spacecraft. This paper also shows that noise in relative velocity measurements plays a major roll in fleet performance. The author [1] mentions that to maintain a fleet of spacecraft in a formation, a regular on-board correction is required. The need for regular correction of the spacecraft fleet results in more fuel per satellite will be used than for a single satellite. This requires higher amount of on-board fuel or a high degree of confidence must be placed in a fuel-minimizing control systems.

1.2 Statement of contribution

Our contributions may be summarized in the derivation, implementation (in a simulation environment) and comparison of different Model Predictive Control (MPC) strategies that guarantee satellites to follow a pre-specified formation.

We indeed present several control approach methods for constructing and maintaining a formation in orbit and show methods that are more suitable for on-board fuel usage reduction.

We moreover present a tailored stochastic MPC version of the controllers above that accounts for uncertainty on the thrust inputs, and renders the overall regulation strategy more robust to such disturbances.

1.3 Organization of the thesis

Chapter 2 introduces the mechanical frames that are used to express navigation in space, and to describe orbits of satellites. Chapter 3 presents the derivation of the equation of motion through enumerating and describing the effects of that governing forces that affect the movement of satellites in orbit and the relative dynamics. Chapter 4 presents the linearization of these dynamics, with the aim of deriving models for the motion that are suitable for deriving Linear Quadratic Regulator (LQR) and MPC regulation strategies. Chapter 5 introduces formally the main control problem, plus presents different control formulations. The same chapter moreover presents some tests of how the different control strategies behave, and searches the most efficient control strategy for the current problem. Chapter 6 eventually considers a robust implementation of the control problem, more precisely a scenario based MPC, so to account for both additive noises and parametric uncertainties. Ancillary mathematical derivations are eventually left in the Appendix.

Chapter 2

The multibody description

2.1 Earth's frame

We start by constructing reference points to be able to navigate in space. As satellites will be orbiting Earth, one of the reference points can be positioned at the center of the Earth and we can create a frame around this point using it as the origin. To simplify calculations, we would also like a frame that is stationary with respect to satellites. For this propose we will use the Earth-centered inertial (ECI) frame illustrated in Figure 2.1. In this thesis we will use notion $\mathcal{E}$ (Earth) for indicating the ECI frame. $\mathcal{E}$'s fundamental plane lies at the equator, while its origin is located at the center of the Earth as mentioned before. The three axes are defined by three unit vectors:

- $\widehat{\boldsymbol{I}}$, directed from the Earth's center along the vernal equinox [1];
- $\widehat{\boldsymbol{K}}$, normal to the fundamental (Equatorial) plane and positive in the direction of the geographic north pole;
- $\widehat{\boldsymbol{J}}$, completing $\widehat{\boldsymbol{I}}$ and $\widehat{\boldsymbol{K}}$ so to form a right-handed basis for $\mathbb{R}^3$.

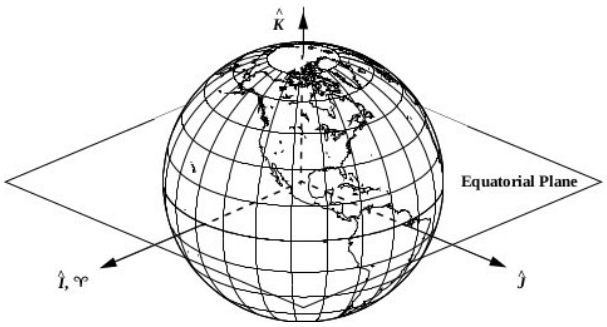

Figure 2.1: Earth-centered inertial (ECI) [4]. This system uses the Earth's equator and the axis of rotation to define an orthogonal set of vectors. The vernal equinox direction is fixed at a specific epoch for most applications.

[1] An equinox occurs when the Earth is at a position in its orbit such that a vector from the Earth towards the sun points to where the ecliptic intersects the celestial equator. The vernal equinox occurs near the first day of spring.

2.2 Local frame

We define an additional reference frame with well defined properties that is local w.r.t. the space debris and the satellites surrounding it. The system of choice is the Gaussian coordinate system or also known as Local Vertical Local Horizontal (LVLH) frame that moves with our formation of satellites. The LVLH frame is illustrated in Figure 2.2 and the origin of LVLH frame is placed at the center of mass of a debris satellite. The $\widehat{\boldsymbol{x}}$ axis will always points out from the debris satellite along the Earth's radius vector to the satellite as it moves in orbit. This rotating frame with three axes is defined by following unit vectors:

1. $\widehat{\boldsymbol{x}}$, directed from the spacecraft's center of mass radially outward
2. $\widehat{\boldsymbol{z}}$, normal to the fundamental plane and positive in the direction of the (instantaneous) angular momentum vector
3. $\widehat{\boldsymbol{y}}$, in a circular orbit, this axis points in the direction of the velocity vector.

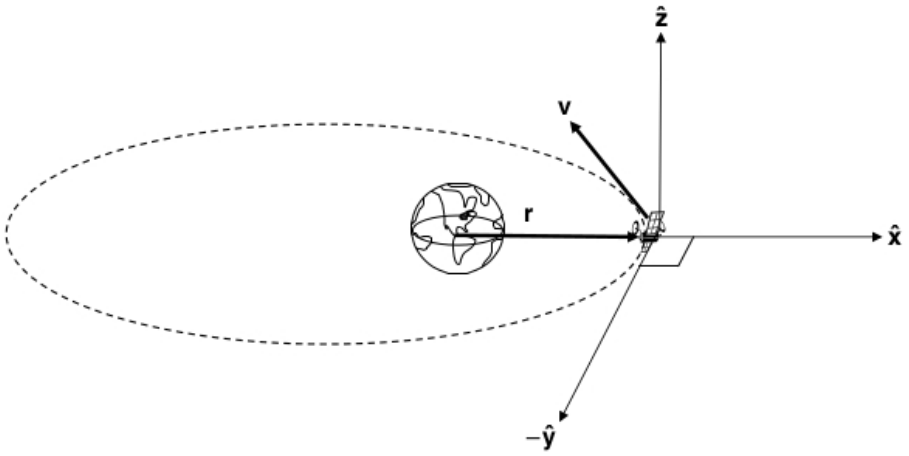

Figure 2.2: Local-vertical, Local-horizontal rotating coordinate system. Origin is positioned at center of mass of the debris spacecraft. The unit vector $\hat{\boldsymbol{x}}$ is directed from the spacecraft radially outward [1].

As $\widehat{\boldsymbol{x}}$ is always pointing radially outwards, this implies that the LVLH frame will rotate as it moves along the orbit. After a full orbit, the LVLH frame will have finished a 360 degree turn around its axis, thus making the angular velocity of LVLH frame equal to satellites angular velocity around Earth.

2.3 Problem description

Lets assume that the space debris of interest is an old satellite that needs to be removed from a LEO. The debris satellite has its front, rear, top and bottom that can be represented with a frame $\mathcal{S}_0$. As the satellite formation will approach the debris satellite, it is reasonable to place origin of the LVLH frames at debris satellites center of mass as mentioned in chapter 2.2. We assume that debris satellites attitude is aligned with LVLH frames axis and its attitude will not

change with time, thus whenever something will be referred to LVLH frame, it will also apply for the debris satellites $\mathcal{S}_0$ frame. The submersion of $\mathcal{S}_0$ and LVLH frames is illustrated in Figure 2.3.

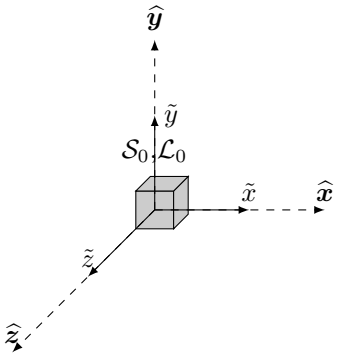

Figure 2.3: The Local Vertical Local Horizontal (LVLH) frame and altitude frame of the debris satellite. The origin of the LVLH frame is positioned at the center of mass of the debris satellite.

To approach the debris, a satellite will use its thrusters to produce force in a desired direction. As the mass of the satellite is known, the acceleration that the satellite will be experiencing due to its thrusters is known as well. For satellite formation control, we need to know how the thrusters affect the motion of the satellites in orbit once they are approaching the debris. To derive the relative acceleration we need to relate the ECI and LVLH frames. We thus assume following:

1. the debris, indicated with s_0, orbits Earth at a constant angular velocity n_0;
2. the angle of the reference frame LVLH with respect to frame $\mathcal{E}$ is $\boldsymbol{\theta}$ and $\left|\dot{\boldsymbol{\theta}}\right| = n_0$;
3. the debris satellite is in a circular orbit, thus in the debris satellite frame the Earth is fixed, namely the $\left|\dot{\boldsymbol{r}}_{\mathcal{E}}^{\mathcal{L}}\right| = 0$;
4. the additional satellite chasing the debris, indicated with s_1, has its position and velocity defined by the quantities:
   - $\boldsymbol{r}_1^{\mathcal{E}}$, the position vector of s_1 in the reference frame $\mathcal{E}$;
   - $\boldsymbol{r}_{\mathcal{L}}^{\mathcal{E}}$, the position vector of the LVLH frame $\mathcal{L}$ in the reference frame $\mathcal{E}$;
   - $\boldsymbol{\rho}_1^{\mathcal{L}}$, the position vector of s_1 in the LVLH frame $\mathcal{L}$.

All previous assumptions and notions are represented in Figure 2.4. This representation will be used to derive the governing equations of motion Chapter 3.

We stress that in our assumptions the debris s_0 is in circular orbit and that, initially, also the chasing satellite s_1 will have a circular orbit. It is important to know the orbit of the debris satellite, because from orbit description we can obtain its state (namely the position and its velocity in the $\mathcal{E}$ frame). A generic orbit description is illustrated in Figure 2.5.

In our analysis we will assume that the debris s_0 will follow the orbital parameters in Table 2.1 and the debris satellite moves in the direction of Earth's rotation and the altitude is measured from the sea level on Earth. i is the inclination of the orbit and it is represented in Figure 2.5.

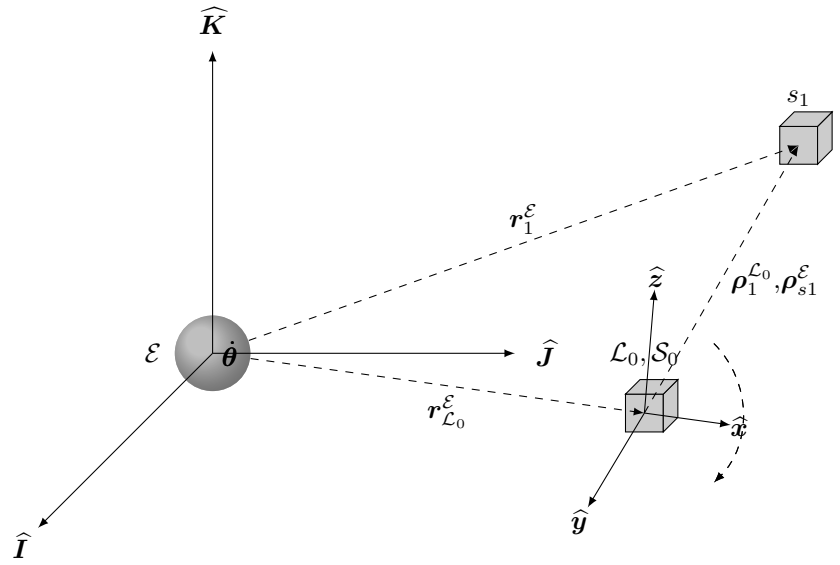

Figure 2.4: Graphical representation of the ECI ($\mathcal{E}$), LVLH ($\mathcal{L}$) and debris satellites frame $\mathcal{S}_0$. Debris satellites frame $\mathcal{S}_0$ lies on the LVLH frame $\mathcal{L}$ and has the same origin. For formation control, we will consider that frame $\mathcal{S}_0$ is aligned with $\mathcal{L}$ and has identical position and attitude at all times. The figure also shows the distances to satellites in the origin of the $\mathcal{E}$ frame and the relative distance in the $\mathcal{L}$ frame as dashed lines.

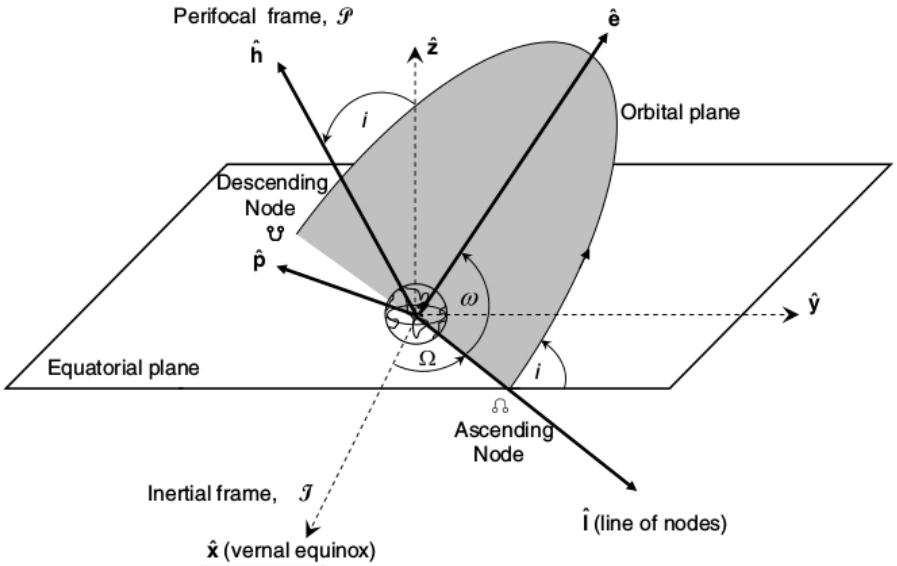

Figure 2.5: Orbit description [1]. Definition of the classical orbital elements: The RAAN Ω, the argument of periapsis ω, and the inclination i.

Name	*Notation*	*Value / Property*	*Units*
Altitude	a_0	300	$[km]$
Inclination	i	45	deg
Right ascension of the ascending node	Ω	0	deg
Eccentricity	e	0	–
Direction	–	Prograde	–

Table 2.1: Orbital parameter notations. Inclination shows how much is the debris satellites orbital frame tilted from the equatorial plane. The right ascension of the ascending node shows how much is the orbital plane is rotated around $\hat{K}$ axis. Eccentricity shows how much does an orbit is deviated from a perfect circle. Additional parameters as semi-major, semi-minor, are not added, because they are not defined for a circular orbit. The argument of perigee and true anomaly are not defined for circular orbit as well. In our case, RAAN is equal to zero, thus $\hat{I}$ is aligned wit the vernal equinox axis.

Chapter 3

Equations of motion

This section focuses on obtaining a state space model, i.e., a state-space description of the differential equations governing the motion of the satellites [8]. This description will then be essential to formulate precisely the satellites formation control problem.

To obtain the state-space description we will describe which forces are acting on a generic satellite in orbit. For defining the control problem we will also derive the properties of the relative accelerations among satellites. Finding analytically the behavior of the relative accelerations is a crucial step in controlling the satellites, as we will use thrusters to maneuver in space and thrusters affect satellite acceleration. In other words, we need to know how will thrusters affect satellites in orbit and with this information we will be able to predict the paths of the satellites.

3.1 Orbital dynamics for a satellite

Figure 3.1 represents a general set-up of a satellite s_1 and a debris s_0 in orbit. Here $\boldsymbol{F}_1^{\mathcal{E}}$ and $\boldsymbol{F}_0^{\mathcal{E}}$ indicate the (vectorial) forces acting acting on s_1 and s_0 respectively. Recall that the LVLH frame is centered in the debris' center of mass, as mentioned in Chapter 2.2. The relative force between satellites can be expressed with $\boldsymbol{F}_1^{\mathcal{L}}$ or with two following vectors,

$$\boldsymbol{F}_1^{\mathcal{L}} = \boldsymbol{F}_1^{\mathcal{E}} - \boldsymbol{F}_0^{\mathcal{E}}.$$

Moreover $\dot{\boldsymbol{\theta}}$ is the angular velocity of the LVLH frame.

3.1.1 Gravitational force

We start considering what are the velocity conditions for a circular orbit. In first approximation, assuming that Earth is a point mass, we have the Newtons gravitational law

$$F_g = -\frac{Gm_{\oplus}m_i}{r^2} \tag{3.1}$$

and it works as a centripetal force. The centrifugal force expression is

$$F_c = m_i r n_0^2, \tag{3.2}$$

where n_0 is the satellites angular velocity in a circular orbit. To make satellites maintain a circular orbit, these two forces should cancel out each other, namely

$$\frac{Gm_{\oplus}m_{\text{sat}}}{r^2} = m_{\text{sat}} r n_0^2. \tag{3.3}$$

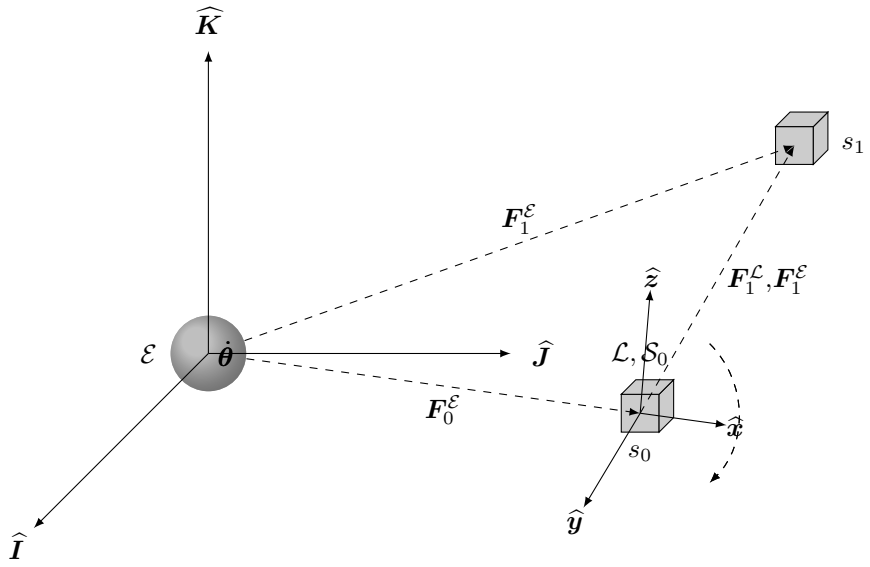

Figure 3.1: Graphical representation of two satellites in the ECI frame. The dashed lines represent the gravitational force acting on satellites and also the relative force between the satellites. The $\mathcal{L}$ frame has rotational velocity equal to $\dot{\theta}$.

By simplifying we obtain following angular velocity around the Earth

$$n_0 = \sqrt{\frac{\mu}{r^3}}. \tag{3.4}$$

We then consider that the gravitational force acting on a generic satellite s_i in the Earth's frame, denoted as $F_i^{\mathcal{E}}$, is

$$\boldsymbol{F}_i^{\mathcal{E}} = m_i \boldsymbol{a}_i^{\mathcal{E}} = -\frac{G m_\oplus m_i}{\left|\boldsymbol{r}_i^{\mathcal{E}}\right|^2} \frac{\boldsymbol{r}_i^{\mathcal{E}}}{\left|\boldsymbol{r}_i^{\mathcal{E}}\right|}, \qquad i = 0, 1, \ldots, \tag{3.5}$$

where $\dfrac{\boldsymbol{r}_i^{\mathcal{E}}}{\left|\boldsymbol{r}_i^{\mathcal{E}}\right|}$ is a unit vector added for indicating the direction of the force. Recalling from Figure 2.4 that $\boldsymbol{r}_1^{\mathcal{E}} = \boldsymbol{r}_0^{\mathcal{E}} + \boldsymbol{\rho}_1^{\mathcal{L}}$, we can immediately derive from (3.5) the acceleration for s_1 as

$$\boldsymbol{a}_1^{\mathcal{E}} = -\frac{G m_\oplus}{\left|\boldsymbol{r}_1^{\mathcal{E}}\right|^2} \frac{\boldsymbol{r}_1^{\mathcal{E}}}{\left|\boldsymbol{r}_1^{\mathcal{E}}\right|} = -\frac{G m_\oplus}{\left|\boldsymbol{r}_0^{\mathcal{E}} + \boldsymbol{\rho}_1^{\mathcal{L}}\right|^2} \frac{\boldsymbol{r}_0^{\mathcal{E}} + \boldsymbol{\rho}_1^{\mathcal{L}}}{\left|\boldsymbol{r}_0^{\mathcal{E}} + \boldsymbol{\rho}_1^{\mathcal{L}}\right|} \tag{3.6}$$

3.1.2 The J_2 effect

(3.6) is quite approximate: since the Earth's shape is not perfectly spherical, the gravitational field changes during the orbit. Thus, due to Earth's flattening and non-evenly distributed mass, a satellite in orbit will not follow a stationary orbit, as it is usually represented in the two-body assumptions. The effect due to Earth's flattening is split in zonal harmonics [4] and is commonly referred as J_2, J_3 and J_4. These are the zonal coefficients that depend on the latitude, and the J_2 term is by far the most important, being roughly 1000 times greater than either J_3 or J_4. We

use the mathematics proposed in [1] to model the effect of J_2, i.e., assume that

$$\ddot{x}_i^{\mathcal{E}} = -\frac{\mu x_i^{\mathcal{E}}}{r^3}\left[1 - \frac{3}{2}J_2\left(\frac{R_e}{r}\right)^2\left(5\frac{(z_i^{\mathcal{E}})^2}{r^2} - 1\right)\right] \tag{3.7}$$

$$\ddot{y}_i^{\mathcal{E}} = -\frac{\mu y_i^{\mathcal{E}}}{r^3}\left[1 - \frac{3}{2}J_2\left(\frac{R_e}{r}\right)^2\left(5\frac{(z_i^{\mathcal{E}})^2}{r^2} - 1\right)\right] \tag{3.8}$$

$$\ddot{z}_i^{\mathcal{E}} = -\frac{\mu z_i^{\mathcal{E}}}{r^3}\left[1 - \frac{3}{2}J_2\left(\frac{R_e}{r}\right)^2\left(5\frac{(z_i^{\mathcal{E}})^2}{r^2} - 3\right)\right]. \tag{3.9}$$

These equations are represented in the Earth's frame $\mathcal{E}$; Figure 3.2 shows the J_2 effect on a single satellite in orbit. The shadow on $\hat{K}$ and $\hat{J}$ side of this plot shows that the RAAN is affected due to the J_2 effect. In addition, changes in altitude are expected based on shadow plots on the $\hat{K}, \hat{I}$ and $\hat{I}, \hat{J}$ faces. As this figure is in the Earth's frame $\mathcal{E}$, it is difficult to determine exactly how much the J_2 affects the motion of the satellite.

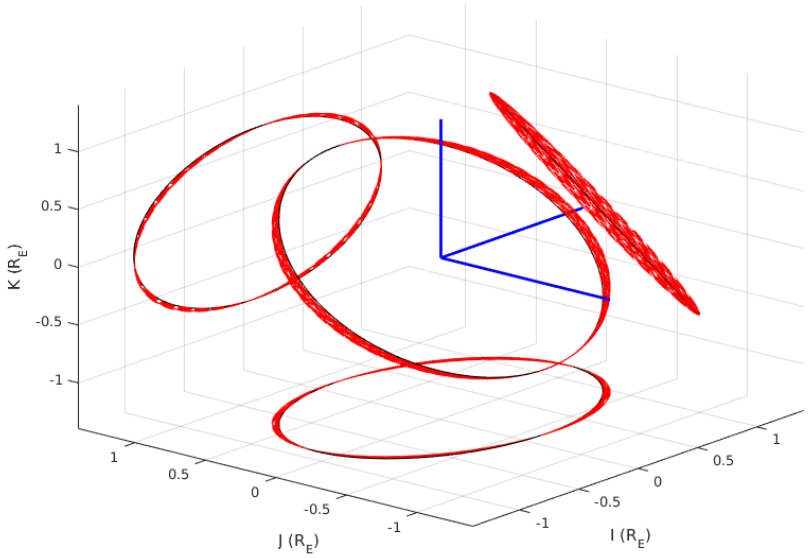

Figure 3.2: The effect of the $J2$ on a single satellite in orbit. The units of the plot is one Earth radius or 6371 [km]. $s_0^{\mathcal{E}}(t)$ shows the path that debris satellite took due to the J_2 effect.

Figure 3.3 shows the effect of the J_2 as an argument of altitude. We see that in our scenario the altitude can decrease up to 13 kilometers and that it takes approximately 90 minutes for a satellite to make a complete orbit around the Earth based on the altitude shown in Table 2.1.

To transform the J_2 effects on the local frame we exploit the $R_{\mathcal{E}}^{\mathcal{L}}$ matrix reported in Appendix A.2. $R_{\mathcal{E}}^{\mathcal{L}}$ is a rotation matrix whose transpose will provide us with the necessary transformation of the effect from frame $\mathcal{E}$ to frame $\mathcal{L}$. Notice that this transformation is only valid for circular orbits, because for a circular orbit our velocity vector points in the same direction as the $\mathcal{L}$ frame's y axis, thus we can express $y_{\mathcal{L}}$ as $\frac{v}{|v|}$. When considering an elliptic orbit then the $\frac{v}{|v|}$

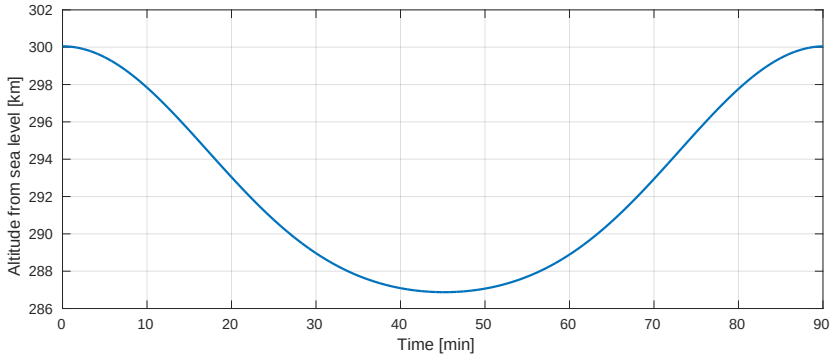

Figure 3.3: Changes in altitude during a full orbit. During one orbit a satellite decreased its altitude up to 13 kilometers. The altitude in this graph is represented as $s^{\mathcal{E}}_{0alt}$ and it is measured from the sea level on the Earth.

vector does not point in the same direction as the $y^{\mathcal{L}}$ axis of the LVLH frame, and thus this transformation will not be valid trough out the orbit.

3.2 Relative orbital dynamics

The relative acceleration between the debris s_0 and the chasing satellite s_1 is expressed by the difference between their acceleration vectors. From (3.5) and (3.6), thus, it follows that

$$\frac{d^2}{dt^2}\boldsymbol{\rho}_1^{\mathcal{E}} = -\frac{Gm_\oplus}{\left|\boldsymbol{r}_0^{\mathcal{E}} + \boldsymbol{\rho}_1^{\mathcal{L}}\right|^2}\frac{\boldsymbol{r}_0^{\mathcal{E}} + \boldsymbol{\rho}_1^{\mathcal{L}}}{\left|\boldsymbol{r}_0^{\mathcal{E}} + \boldsymbol{\rho}_1^{\mathcal{L}}\right|} + \frac{Gm_\oplus}{\left|\boldsymbol{r}_0^{\mathcal{E}}\right|^2}\frac{\boldsymbol{r}_0^{\mathcal{E}}}{\left|\boldsymbol{r}_0^{\mathcal{E}}\right|}. \tag{3.10}$$

Since the controller developed later in the thesis will consider equations expressed only in the local frame $\mathcal{L}$ it is necessary to transform the term $\frac{d^2}{dt^2}\boldsymbol{\rho}_1^{\mathcal{E}}$ into something relative to the $\mathcal{L}$ frame. By using the derivations in Appendix A.1, we substitute (A.15) into (3.10) and rename $Gm_\oplus$ with μ. We thus transform (3.10) into

$$\frac{d^2}{dt^2}\boldsymbol{\rho}_1^{\mathcal{L}} + 2(\dot{\boldsymbol{\theta}} \times \frac{d}{dt}\boldsymbol{\rho}_1^{\mathcal{L}}) + \frac{d}{dt}\dot{\boldsymbol{\theta}} \times \boldsymbol{\rho}_1^{\mathcal{L}} + \dot{\boldsymbol{\theta}} \times (\dot{\boldsymbol{\theta}} \times \boldsymbol{\rho}_1^{\mathcal{L}}) = -\frac{\mu}{\left|\boldsymbol{r}_0^{\mathcal{E}} + \boldsymbol{\rho}_1^{\mathcal{L}}\right|^2}\frac{\boldsymbol{r}_0^{\mathcal{E}} + \boldsymbol{\rho}_1^{\mathcal{L}}}{\left|\boldsymbol{r}_0^{\mathcal{E}} + \boldsymbol{\rho}_1^{\mathcal{L}}\right|} + \frac{\mu}{\left|\boldsymbol{r}_0^{\mathcal{E}}\right|^2}\frac{\boldsymbol{r}_0^{\mathcal{E}}}{\left|\boldsymbol{r}_0^{\mathcal{E}}\right|}. \tag{3.11}$$

(3.11) will then be used to control satellites in orbit. Our goal is now to obtain a state space representation of this equation; but since this is a non-linear differential equation, we need to perform a linearization step before.

Chapter 4

Linearization and State-Space form

We divide the problem in two parts: first deriving the linearized equations of motion in continuous time, and then derive a discrete equivalent representation of them, that is useful for deriving our consequent MPC strategies.

4.1 Continuous time

We now break down the equation of motion (3.11) into the separate dimensions x, y and z of the local frame $\mathcal{L}$. Letting then

$$\boldsymbol{\rho}_1^{\mathcal{L}} := \begin{bmatrix} x & y & z \end{bmatrix}^T$$

and (recalling that the local frame is by definition rotating around the local z)

$$\dot{\boldsymbol{\theta}} := \begin{bmatrix} 0 & 0 & \dot{\theta}_0 \end{bmatrix}^T,$$

equation (3.11) becomes

$$\begin{bmatrix} \ddot{x} \\ \ddot{y} \\ \ddot{z} \end{bmatrix} + 2 \begin{bmatrix} -\dot{\theta}_0 \dot{y} \\ -\dot{x}\dot{\theta}_0 \\ 0 \end{bmatrix} + \begin{bmatrix} -y\ddot{\theta}_0 \\ \ddot{\theta}_0 x \\ 0 \end{bmatrix} + \begin{bmatrix} \dot{\theta_0}^2 x \\ -\dot{\theta_0}^2 x \\ 0 \end{bmatrix} = -\frac{\mu}{\left|\boldsymbol{r}_0^{\mathcal{E}} + \boldsymbol{\rho}_1^{\mathcal{L}}\right|^2} \frac{\boldsymbol{r}_0^{\mathcal{E}} + \boldsymbol{\rho}_1^{\mathcal{L}}}{\left|\boldsymbol{r}_0^{\mathcal{E}} + \boldsymbol{\rho}_1^{\mathcal{L}}\right|} + \frac{\mu}{\left|\boldsymbol{r}_0^{\mathcal{E}}\right|^2} \frac{\boldsymbol{r}_0^{\mathcal{E}}}{\left|\boldsymbol{r}_0^{\mathcal{E}}\right|}. \tag{4.1}$$

Replacing $\boldsymbol{\rho}_1^{\mathcal{L}}$ with $\begin{bmatrix} x & y & z \end{bmatrix}^T$ also in the right-hand side, and splitting the resulting equation into the three separate components then leads to

$$\ddot{x} - 2\dot{\theta}_0\dot{y} - \ddot{\theta}_0 y - \dot{\theta_0}^2 x = -\frac{\mu}{\left((\left|\boldsymbol{r}_0^{\mathcal{E}}\right| + x)^2 + y^2 + z^2\right)^{3/2}} \left(\left|\boldsymbol{r}_0^{\mathcal{E}}\right| + x\right) + \frac{\mu}{\left|\boldsymbol{r}_0^{\mathcal{E}}\right|^2} \tag{4.2}$$

$$\ddot{y} + 2\dot{\theta}_0\dot{x} + \ddot{\theta}_0 x - \dot{\theta_0}^2 y = -\frac{\mu y}{\left((\left|\boldsymbol{r}_0^{\mathcal{E}}\right| + x)^2 + y^2 + z^2\right)^{3/2}} \tag{4.3}$$

$$\ddot{z} = -\frac{\mu z}{\left((\left|\boldsymbol{r}_0^{\mathcal{E}}\right| + x)^2 + y^2 + z^2\right)^{3/2}} \tag{4.4}$$

Notice then that:

1. $\left|\boldsymbol{r}_0^{\mathcal{E}}\right|$ is aligned with the x direction, as stated in Chapter 2.2;
2. the equations of motion above are simplified in the sense that they do not include the J_2 effects; corrections will then performed in Chapter 4.2;
3. in the current model our orbit is chosen to be circular and this implies that the radius of an orbit will not change, thus $\left|\boldsymbol{r}_0^{\mathcal{E}}\right|$ is a constant value, say a_0. For the same reason the local frame $\mathcal{L}$ is rotating with a constant angular velocity $\dot{\boldsymbol{\theta}}$, and this value can then be replaced with the constant value n_0. Moreover $\ddot{\theta} = 0$.

Considering the notes above we can rewrite (4.2) as

$$\ddot{x} - 2n_0\dot{y} - n_0^2 x = -\frac{\mu}{\Big((a_0+x)^2+y^2+z^2\Big)^{3/2}}\big(a_0+x\big) + \frac{\mu}{a_0^2} \tag{4.5}$$

$$\ddot{y} + 2n_0\dot{x} - n_0^2 y = -\frac{\mu y}{\Big((a_0+x)^2+y^2+z^2\Big)^{3/2}} \tag{4.6}$$

$$\ddot{z} = -\frac{\mu z}{\Big((a_0+x)^2+y^2+z^2\Big)^{3/2}}. \tag{4.7}$$

As mentioned before, equations (4.5) to (4.7) are non-linear; to derive computationally inexpensive control algorithms we then proceed to linearize these equations. Linearization of the right hand side for expressions (4.5) to (4.7) is then done by an opportune first-order Taylor expansion around the origin of the LVLH frame, so that (4.5) is linearized with respect to x, (4.6) with respect to y and (4.7) with respect to z. After this operation we obtain the following set of equations:

$$\ddot{x} - 2n_0\dot{y} - 3n_0^2 x = 0 \tag{4.8}$$

$$\ddot{y} + 2n_0\dot{x} = 0 \tag{4.9}$$

$$\ddot{z} + n_0^2 z = 0. \tag{4.10}$$

Equations (4.8) to (4.10) are called the Clohessy-Wiltshire (CW) equations [1]. They represent the relative motion of a satellite in orbit with respect to the $\mathcal{L}$ frame. Additionally, acceleration can be affected by on-board thrusters and additional disturbances, thus we can add these components to the CW equations and obtain the linearized representation of the relative motion.

$$\ddot{x} - 2n_0\dot{y} - 3n_0^2 x = u_x + d_x \tag{4.11}$$

$$\ddot{y} + 2n_0\dot{x} = u_y + d_y \tag{4.12}$$

$$\ddot{z} + n_0^2 z = u_z + d_z \tag{4.13}$$

(4.11) to (4.13) can then be transformed in the following state-space form,

$$\dot{\boldsymbol{x}} = A\boldsymbol{x} + B\boldsymbol{u} + F\boldsymbol{d}, \tag{4.14}$$

where

$$A = \begin{bmatrix} 0 & 0 & 0 & 1 & 0 & 0 \\ 0 & 0 & 0 & 0 & 1 & 0 \\ 0 & 0 & 0 & 0 & 0 & 1 \\ 3n_0^2 & 0 & 0 & 0 & 2n_0 & 0 \\ 0 & 0 & 0 & -2n_0 & 0 & 0 \\ 0 & 0 & -n_0^2 & 0 & 0 & 0 \end{bmatrix}$$

$$B = \begin{bmatrix} 0 & 0 & 0 \\ 0 & 0 & 0 \\ 0 & 0 & 0 \\ 1/m_i & 0 & 0 \\ 0 & 1/m_i & 0 \\ 0 & 0 & 1/m_i \end{bmatrix}, F = \begin{bmatrix} 0 & 0 & 0 \\ 0 & 0 & 0 \\ 0 & 0 & 0 \\ 1 & 0 & 0 \\ 0 & 1 & 0 \\ 0 & 0 & 1 \end{bmatrix}$$

$$\boldsymbol{x} = \begin{bmatrix} x \\ y \\ z \\ \dot{x} \\ \dot{y} \\ \dot{z} \end{bmatrix}, \boldsymbol{u} = \begin{bmatrix} u_x \\ u_y \\ u_z \end{bmatrix}, \boldsymbol{d} = \begin{bmatrix} d_x \\ d_y \\ d_z \end{bmatrix}.$$

Above, $\boldsymbol{x}$ is the state of a particular satellite, while the B matrix expresses the thruster effect on the satellite (that, by Newtons law of acceleration, is equal to the force generated by the thrusters divided by the mass of the object). Notice thus that the dimension of our input $\boldsymbol{u}$ will be in Newton $[N]$.

Before proceeding we should check the effects of the linearization step, and thus compare the linearized and the non-linear models. Namely we now perform a comparison between Equations (4.2) - (4.4) and (4.8) - (4.10). This comparison aims at showing the accuracy of the linearized model by placing a satellite in a different positions in the LVLH frame, and check how much the trajectories of the linearized model deviate from the ones obtained using the original non-linear model. Integration of the position error is shown in Figure 4.1, where the satellite has been placed on the x and y plane on the LVLH frame.

From the numerical simulations we see that even 1 kilometre away from the origin of the LVLH frame, the absolute error committed by using the linearized motion would only be 65 cm. To be precise, we assume that during these 16 minutes the satellite did not encounter any disturbance; but nonetheless in our scheme the various satellites will be constantly controlled with help of control algorithms, thus we will only experience only small effects due to linearization errors. Additionally we see in Figure 4.1 that close to the origin the error is very small, and this makes the approximation more accurate when working around the origin of the LVLH frame. We thus eventually conclude that the linearization performed in this chapter seems to be a valid assumption for modelling relative motion of satellites.

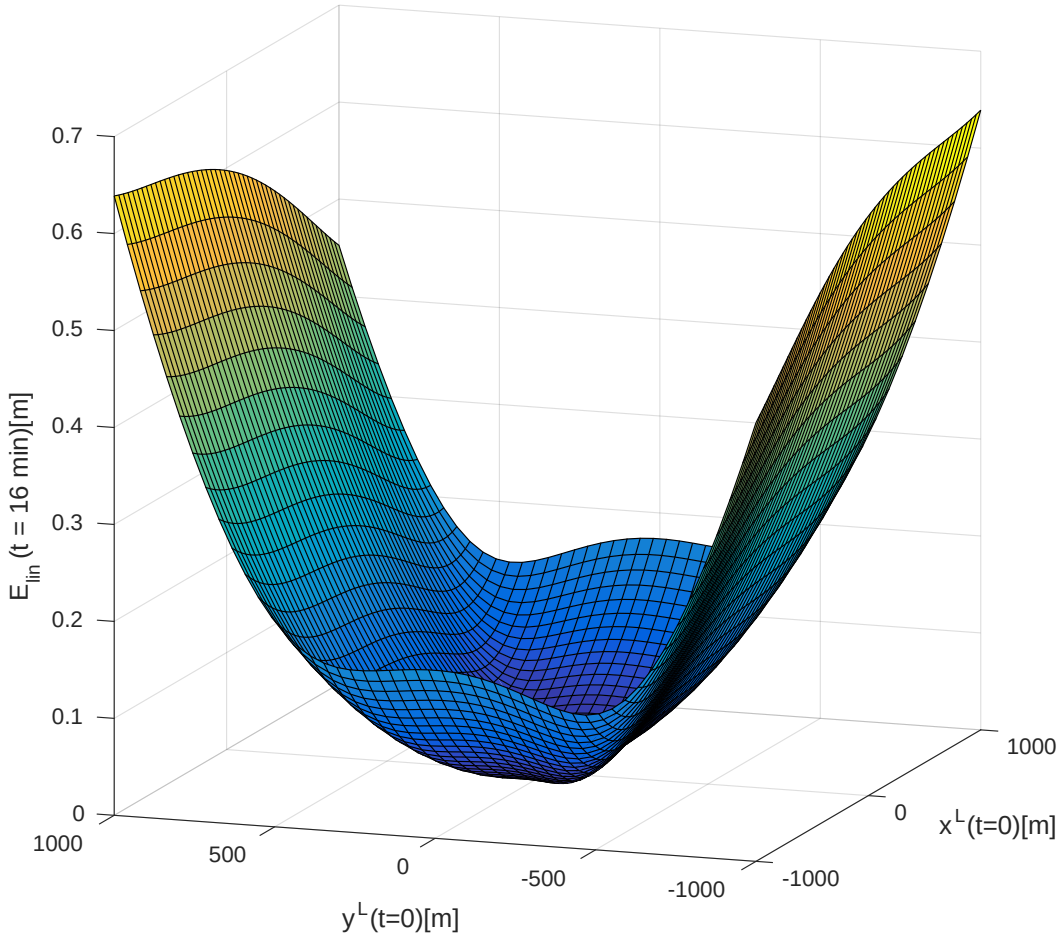

Figure 4.1: Error due to the linearization step. At time equal zero, a satellite was placed in a certain position on x, y axis of the LVLH plane. In the ordinate of the figure E_{lin} shows the distance in meters between the trajectories obtained using the linear and non-linear models. More specificaly we place satellites in the same positions in the LVLH plane at time zero, let them drift in free space, and then compute the absolute error between their positions after 16 minutes.

4.2 Linearized J_2 -differential equation for circular orbits

We here present (without derivations, that can be found in [1]) the linearized equations for motions that are perturbed by mean drifts due to J_2 plus short-periodic effects. The novel state-update matrix is in this case

$$A^{J2} = \begin{bmatrix} 0 & 0 & 0 & 1 & 0 & 0 \\ 0 & 0 & 0 & 0 & 1 & 0 \\ 0 & 0 & 0 & 0 & 0 & 1 \\ a_{41} & a_{42} & a_{43} & 0 & 2\alpha_z & 0 \\ a_{51} & a_{52} & a_{53} & -2\alpha_z & 0 & 2\alpha_x \\ a_{61} & a_{62} & a_{63} & 0 & -2\alpha_x & 0 \end{bmatrix} \tag{4.15}$$

where

$$a_{41} := \alpha_z^2 + 2\frac{\mu}{r_0^3} + \gamma\Big(1 - 3\sin^{-1}(i_0)^2 sin^{-1}(\omega_0)^2\Big)$$

$$a_{42} := \dot{\alpha}_z + \gamma\Big(\sin^{-1}(i_0)^2 \sin^{-1}(2\omega_0)\Big)$$

$$a_{43} := -\alpha_x\alpha_z + \gamma\Big(\sin^{-1}(2i_0)\sin^{-1}(\omega_0)\Big)$$

$$a_{51} := -\dot{\alpha}_z + \gamma\Big(sin^{-1}(i_0)^2 \sin^{-1}(2\omega_0)\Big)$$

$$a_{52} := \alpha_x^2 + \alpha_z^2 - \frac{\mu}{r_0^3} + \gamma\Big(-\frac{1}{4} + \sin^{-1}(i_0)^2\Big(\frac{7}{4}sin^{-1}(\omega_0)^2 - \frac{1}{2}\Big)\Big)$$

$$a_{53} := \dot{\alpha}_x + \gamma\Big(-\frac{1}{4}\sin^{-1}(2i_0)\cos^{-1}(\omega_0)\Big)$$

$$a_{61} := -\alpha_x\alpha_z + \gamma\Big(\sin^{-1}(2i_0)\sin^{-1}(\omega_0)\Big)$$

$$a_{62} := 0$$

$$a_{63} := \alpha_x^2 - \frac{\mu}{r_0^3} + \gamma\Big(\frac{-3}{4} + \sin^{-1}(i_0)^2\Big(\frac{5}{4}\sin^{-1}(\omega_0)^2 + \frac{1}{2}\Big)\Big).$$

Matrix (4.15) represents the relative dynamics that include the J_2 effect. As the J_2 effect is dependent on the position of the satellites in space, namely in the $\mathcal{E}$ frame, this implies that the A^{J2} matrix needs to be recomputed as the satellite propagates. To compute all the coefficients inside matrix A^{J2}, we need to estimate ω_0 (i.e., the argument of the latitude, represented as ω in Figure 2.5 in Chapter 2.3). The argument of latitude ω_0 can then be estimated with the help of a vector that is pointing towards the ascending node and a position vector of a satellite in $\mathcal{E}$ frame as in

$$\theta_0 = \cos^{-1}\frac{\langle n, r_0^{\mathcal{E}}\rangle}{|n||r_0^{\mathcal{E}}|}.$$

The vector pointing towards the ascending node is obtained by a cross product between $\boldsymbol{k}$ and $\mathbf{h}$, i.e., as

$$\boldsymbol{n} = \boldsymbol{k} \times \boldsymbol{h}$$

where $\mathbf{h}$ is the specific relative angular momentum of a satellite and $\boldsymbol{k} = \begin{bmatrix} 0 & 0 & 1 \end{bmatrix}$.

Finally, the specific relative angular momentum of a satellite is obtained through

$$\boldsymbol{h} = \boldsymbol{r}_0^{\mathcal{E}} \times \boldsymbol{v}_0^{\mathcal{E}}.$$

As the position $\boldsymbol{r}_0^{\mathcal{E}}$ of a satellite in the $\mathcal{E}$ frame is known, the velocity $\boldsymbol{v}_0^{\mathcal{E}}$ can be estimated. In this way it is possible to obtain all that values that are needed to estimate the dynamics matrix including the J_2 effect.

Additional expressions for (4.15)

$$\dot{\alpha}_x = 0$$

$$\dot{\alpha}_z = 0$$

$$J = J_2\Big(\frac{R_e}{a_0^2}\Big)$$

$$\dot{\omega}_0 = n_0\Big(1 - \frac{3}{2}J\big(1 - 4\cos^{-1}(i_0)^2\big)\Big)$$

$$r_0 = a_0\left[1 + J\left\{\frac{3}{4}\big(1 - 3\cos^{-1}(i_0)^2\big) + \frac{1}{4}\big(\sin^{-1}(i_0)^2\cos^{-1}(2\omega_0)\big)\right\}\right]$$

$$\gamma = 6J_2\Big(\frac{\mu R_e^2}{r_0^5}\Big)$$

$$\dot{\Omega}_0 = \frac{-3}{2}Jn_0\cos^{-1}(i_0)$$

$$\alpha_x = 2\dot{\Omega}_0\sin^{-1}(i_0)\sin^{-1}(\theta_0)$$

$$\alpha_y = 0$$

$$\alpha_z = \dot{\Omega}_0 cos^{-1}(i_0) + \dot{\theta}_0 + \frac{1}{4}Jn_0\cos^{-1}(2\omega_0)sin^{-1}(i_0)^2$$

4.3 Transforming continuous time equations into discrete time ones

Satellites have on-board computers that can control them, but as it is a digital system, it takes some time for a computer to estimate the necessary control input. This implies that our system is working in discrete time and the continuous time model needs to be transformed to discrete time. Even if satellite move at approximately 7 km/s in the $\mathcal{E}$ frame, the relative motion will be much slower around 3.6 km/h, which implies that the on-board computer will have time to compute sophisticated algorithms. We assume that 1 second will be enough to perform these computations, thus we need to transform the continuous time models above based on this assumption.

To this aim we use the linearized continuous dynamics represented in (4.14) excluding disturbances, namely $\dot{\boldsymbol{x}} = A\boldsymbol{x} + B\boldsymbol{u}$. We can set a constant input u to be 1 Newton during 1 second and solve the ordinary differential equation

$$\boldsymbol{x}(t+1) = \int_{t=0}^{t=1} A\boldsymbol{x}(s) + B\boldsymbol{u}(s)ds,$$

where $\boldsymbol{x}(t+1)$ is the state of a satellite after 1 second. So why did we put input equal to 1 Newton? As this is a linear, time-invariant system, the input can be scaled, thus affecting the system linearly. The methods described above is also know as Zero-Order Hold (ZOH).

By using (4.14) and the orbital properties in Chapter 2.3 we eventually obtain the following discrete model of relative satellite dynamics:

$$\boldsymbol{x}(t+1) = A_d\boldsymbol{x}(t) + B_d\boldsymbol{u}(t), \tag{4.16}$$

where

$$A_d = \begin{bmatrix} 1.0000 & 0 & 0 & 1.0000 & 0.0012 & 0 \\ -0.0000 & 1.0000 & 0 & -0.0012 & 1.0000 & 0 \\ 0 & 0 & 1.0000 & 0 & 0 & 1.0000 \\ 0.0000 & 0 & 0 & 1.0000 & 0.0023 & 0 \\ -0.0000 & 0 & 0 & -0.0023 & 1.0000 & 0 \\ 0 & 0 & -0.0000 & 0 & 0 & 1.0000 \end{bmatrix}$$

$$B_d = \begin{bmatrix} 0.0050 & 0.0000 & 0 \\ -0.0000 & 0.0050 & 0 \\ 0 & 0 & 0.0050 \\ 0.0100 & 0.0000 & 0 \\ -0.0000 & 0.0100 & 0 \\ 0 & 0 & 0.0100 \end{bmatrix} /m_i,$$

We can then perform the same discretization procedure for the A^{J2} matrix represented in 4.2; in this case, nonetheless, the discretization needs to be re-calculated for every time step, since the argument of the latitude will change with time.

Chapter 5

Satellite Formation Control

We now propose and compare some different control methods for controlling individual satellites so to maintain a pre-specified formation. We start by defining a LQR, then extend it to become a MPC, and compare when and how the LQR and the MPC perform differently. We will then extend the MPC so to consider some additional limitations on the thrusters and check the effects of J_2 disturbances. Summarizing, thus we will compare different methods of counteracting the disturbances affecting satellites and check which method uses the least amount of on-board propellant to solve the flight control problem.

5.1 Control problem formulation

To develop a control algorithm we first need to formulate the control problem. Assume that we are considering satellite s_i, that we are using bi-propellant thrusters and that our thrusters have a certain pre-specified range plus they are one-directional (i.e., they need to be positioned in front, rear, top, bottom, left and right sides of the satellite). This means that we can split the actuation vector $\boldsymbol{u}_i$ from (4.14) into its positive and negative parts, namely

$$\boldsymbol{u}_i = \begin{bmatrix} u_{x_i^+} & u_{y_i^+} & u_{z_i^+} & u_{x_i^-} & u_{y_i^-} & u_{z_i^-} \end{bmatrix}^T.$$

Correspondingly we update the B in the state-space models as

$$B = \begin{bmatrix} 0 & 0 & 0 \\ 0 & 0 & 0 \\ 0 & 0 & 0 \\ 1/m_i & 0 & 0 \\ 0 & 1/m_i & 0 \\ 0 & 0 & 1/m_i \end{bmatrix} \Rightarrow B = \begin{bmatrix} 0 & 0 & 0 & 0 & 0 & 0 \\ 0 & 0 & 0 & 0 & 0 & 0 \\ 0 & 0 & 0 & 0 & 0 & 0 \\ 1/m_i & 0 & 0 & -1/m_i & 0 & 0 \\ 0 & 1/m_i & 0 & 0 & -1/m_i & 0 \\ 0 & 0 & 1/m_i & 0 & 0 & -1/m_i. \end{bmatrix} \tag{5.1}$$

At this point we have obtained all the necessary mathematical models to create a control algorithm. In this Chapter we will consider two path estimation tactics an compare them to each other.

Formation controlled so to be always referring to the origin of the LVLH frame: Figure 5.1 represents a potential way of describing a satellite formation control problem. In words, we would like the position $\boldsymbol{x}_i$ of each satellite s_i to be a certain pre-specified desired position $\boldsymbol{r}_i$ in the LVLH frame. Indirectly, we would like also to maintain a certain distance

between satellites, namely $\boldsymbol{x}_{ij} - \boldsymbol{r}_{ij}$, even if s_i and s_j are not in their desired positions. To define the optimization problem we consider then the following desired feature: minimize the force applied by the various thrusters (which is in first approximation linearly proportional to used fuel) to enforce the various satellites to be in the previously specified positions and relative distances.

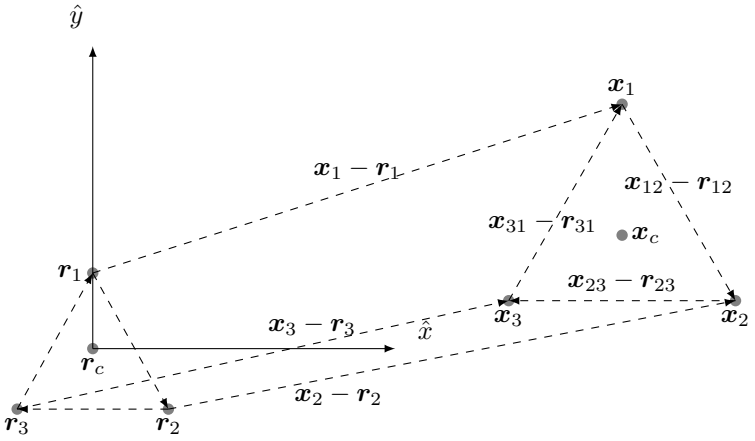

Figure 5.1: General representation of formation. $\boldsymbol{x}_i$ represents position vector of the i satellite and $\boldsymbol{x}_{ij}$ is the relative position vector between satellites i and j, where $i \in \{1...3\}$ and $j \in \{1...3\}$. $\boldsymbol{c}$ is the position vector of the center of formation with respect to LVLH origin.

In math, thus, we seek to solve, for each time instant t,

$$\begin{aligned}
\text{minimize} \quad & \sum_{k=t}^{N} \left(\sum_{i=1}^{3} \left[||\boldsymbol{x}_i(k) - \boldsymbol{r}_i||_Q^2 + ||\boldsymbol{u}_i(k)||_R^2 \right] + \gamma \sum_{j \neq i} ||\boldsymbol{x}_i(k) - \boldsymbol{x}_j(k) - \boldsymbol{r}_{ij}||_{Q'}^2 \right) \\
\text{subject to:} \quad & \boldsymbol{x}_i^+ = A_d \boldsymbol{x_i} + B_d \boldsymbol{u_i} \qquad i, j \in \{1, 2, 3\} \\
& \boldsymbol{x}_i = \begin{bmatrix} x_i & y_i & z_i & \dot{x}_i & \dot{y}_i & \dot{z}_i \end{bmatrix}^T, \\
& \boldsymbol{u}_i = \begin{bmatrix} u_{x_i^+} & u_{y_i^+} & u_{z_i^+} & u_{x_i^-} & u_{y_i^-} & u_{z_i^-} \end{bmatrix}^T
\end{aligned} \quad , \tag{5.2}$$

where:

- $\boldsymbol{x}_i$ is the state of satellite s_i, i.e., its position in frame $\mathcal{L}$;
- $\boldsymbol{r}_i$ is a time-invariant the reference position for s_i in frame $\mathcal{L}$;
- $\boldsymbol{r}_{ij}$ is a time-invariant reference distance vector between s_i and s_j in frame $\mathcal{L}$;
- $||\cdot||_Q^2$, $||\cdot||_{Q'}^2$ and $||\cdot||_R^2$ are opportune norms defined as $\left[\cdot\right] Q \left[\cdot\right]^T$, $\left[\cdot\right] Q' \left[\cdot\right]^T$ and $\left[\cdot\right] R \left[\cdot\right]^T$ respectively; Q, Q' and R are the weighting factors of the designer's choice.
- γ acts as a weight, selected by the designer, that trades off the relative importance of maintaining the formation (the Q' norm) versus maintaining a pre-specified position (the Q norm).

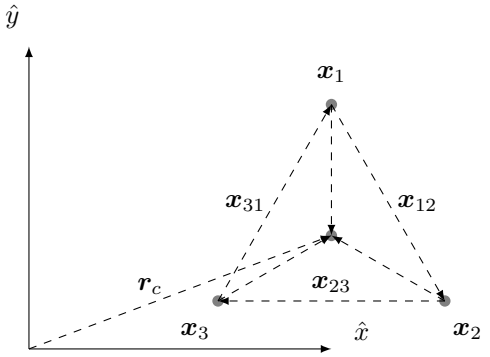

Figure 5.2: General representation of a satellites formation. For each i, $\boldsymbol{x}_i$ represents the position vector of satellite s_i in the $\mathcal{L}$ frame, while $\boldsymbol{x}_{ij}$ denotes the relative position vector between s_i and s_j. $\boldsymbol{c}$ eventually denotes the position vector of the barycenter of the formation in the $\mathcal{L}$ frame.

Formation controlled so to be following a pre-defined path: Figure 5.2 describes an alternative control concept that is similar to the one presented in Figure 5.1, except that in this new case the reference position $\boldsymbol{r}_c$ of the centroid of the satellite formation is moving in time. The novel control problem looks as

$$\begin{aligned}
\text{minimize} \quad & \sum_{k=t}^{N} \left(\sum_{i=1}^{3} \left[||\boldsymbol{x}_i(k) - \boldsymbol{r}'_i(k)||^2_Q + ||\boldsymbol{u}_i(k)||^2_R \right] + \gamma \sum_{j \neq i} ||\boldsymbol{x}_i(k) - \boldsymbol{x}_j(k) - \boldsymbol{r}_{ij}||^2_{Q'} \right) \\
\text{subject to:} \quad & \boldsymbol{x}_i^+ = A_d \boldsymbol{x_i} + B_d \boldsymbol{u_i} \qquad i,j \in \{1,2,3\} \\
& \boldsymbol{x}_i = \begin{bmatrix} x_i & y_i & z_i & \dot{x}_i & \dot{y}_i & \dot{z}_i \end{bmatrix}^T, \\
& \boldsymbol{u}_i = \begin{bmatrix} u_{x_i^+} & u_{y_i^+} & u_{z_i^+} & u_{x_i^-} & u_{y_i^-} & u_{z_i^-} \end{bmatrix}^T
\end{aligned} \quad , \tag{5.3}$$

where

- $\boldsymbol{x}_i$ is the state of satellite s_i, i.e., its position in frame $\mathcal{L}$;
- $\boldsymbol{r}'_i(k)$ is the time varying reference position for satellite s_i in the local frame $\mathcal{L}$. This reference trajectory is updated after every time the main control problem is solved;
- $\boldsymbol{r}_{ij}$ is a time-constant reference distance vector between s_i and s_j in frame $\mathcal{L}$;
- $||\cdot||^2_Q$, $||\cdot||^2_{Q'}$ and $||\cdot||^2_R$ are opportune norms defined as $\left[\cdot\right] Q \left[\cdot\right]^T$, $\left[\cdot\right] Q' \left[\cdot\right]^T$ and $\left[\cdot\right] R \left[\cdot\right]^T$ respectively as before; Q, Q' and R are the weighting factors of the designer's choice.
- γ acts again as a weight, selected by the designer.

The physical meaning of $r'_i(k)$ is that every time the control problem is solved, the control system re-updates an optimal path for the origin of the LVLH frame, and this path can be generated by an optimal LQR control algorithm. If we simulate a single satellite with a LQR controller and save the path that it took, we can then re-use this path as a reference for the formation centroid. More information about the LQR will be introduced in Chapter 5.2 and as well we will discuss some advantages and disadvantages for this method.

5.1.1 Simulation environment

Simulations are performed by tracking the position of each satellite and by computing the acceleration that each satellite is affected by. The orbital dynamics are then described by the Newton's laws and by considering the J_2 effects. The simulation algorithm thus works as follows:

1. consider each satellite's position in the $\mathcal{E}$ frame, i.e., $\boldsymbol{r}_i^{\mathcal{E}}$;
2. decompose it into the components
$$\begin{bmatrix} x_i^{\mathcal{E}} & y_i^{\mathcal{E}} & z_i^{\mathcal{E}} \end{bmatrix}^T$$
3. solve Equation (3.1) to obtain $F_g(\boldsymbol{r}^{\mathcal{E}})$ and thus the acceleration of the satellite due to the gravitational effects ($\frac{d^2}{dt^2}\boldsymbol{r}^{\boldsymbol{\mathcal{E}}} = F_g(\boldsymbol{r}^{\boldsymbol{\mathcal{E}}})$);
4. solve Equations (3.7) to (3.7) to obtain $F_{J2}(\boldsymbol{r}^{\boldsymbol{\mathcal{E}}})$. As discussed in 3.1.2, the point mass assumption is not accurate, so we need to add a correction term that accounts for J_2 effects;
5. obtain the total acceleration that the satellite is experiencing due to Earth in the $\mathcal{E}$ frame, computed as
$$\frac{d^2}{dt^2}\boldsymbol{r}^{\mathcal{E}} = \frac{1}{m_i}\Big(F_g(\boldsymbol{r}^{\mathcal{E}}) + F_{J2}(\boldsymbol{r}^{\mathcal{E}})\Big)$$
6. translate the computed forces to the $\mathcal{L}$ frame by using the transformation matrices $R_{\mathcal{E}}^{\mathcal{L}}$ (A.20)
7. measure the cost of the input by summing up all the input force values for each satellite. To make this output more intuitive, we multiply it by a constant that transforms it from Newtons $[N]$ to kilograms $[kg]$, so that this index refers to the total fuel spent during the simulation.

The algorithm above is used not only to generate Figure 3.2, but also as the main simulation environment for all the future plots. Note that the simulation time horizon might change between different sections of this work; nonetheless, for every specific section the simulation time is constant, so that comparison between different strategies can be done without time-horizon inconsistencies issues.

5.2 Linear quadratic regulator

5.2.1 General LQR Set-up

An effective and widely used control technique for controlling linear time invariant systems design is the so called Linear Quadratic Regulator (LQR) [8]. In this framework the problem is to find a constant state-feedback matrix such that the performance index

$$J = \sum_{k=0}^{\infty} \left(x(k)Qx(k)^T + u(k)Ru(k)^T + 2x(k)Nu(k)^T\right) \tag{5.4}$$

is minimized for the system

$$\boldsymbol{x}(t+1) = A\boldsymbol{x}(t) + B\boldsymbol{u}$$

(where in our case the matrices A and B are taken from Chapter 4). Remarkably, the optimal control sequence minimizing the performance index above is given by

$$u(k) = -K_d(k)x(k)$$

where

$$K_d(k) = (R + BP(k)B^T)^{-1}(B^T P(k)A + N^T)$$

and where P is the unique positive definite solution to the discrete time algebraic Riccati equation

$$P = APA^T - \left(A^T PB + N\right)\left(R + BPB^T\right)^{-1}\left(B^T PA + N^T\right) + Q.$$

See [8] for more details on this particular technique.

5.2.2 LQR performance neglecting J_2 effects

We start by comparing the effect of J_2 on the satellites with simple LQR controller, that does not account for this disturbance. One way to do comparison is to set one simulation environment where Earth's gravity is the only natural acceleration acting on the satellites

$$\frac{d^2}{dt^2}\boldsymbol{r}^{\mathcal{E}} = \frac{1}{m_i}F_g(\boldsymbol{r}^{\mathcal{E}}). \tag{5.5}$$

Figure 5.3 shows the path that was taken in the local frame. At this point satellites get into a formation only when each one of them arrives at the reference position around the origin $\boldsymbol{r}_i^{\mathcal{L}}$. If the initial conditions would be different, there would be a chance of collision on the way from their initial position $\boldsymbol{x}_i(0)$ to the desired point $\boldsymbol{r}_i$. Collision could occur due to the fact that the LQR does not consider the position of the other satellites. This problem is solved in Chapter 5.3 where we will introduce the Model Predictive Control (MPC). The altitude of the debris satellite s_0 does not change due to the lack of J_2 effects as shown in Figure 5.4, thus in the local $\mathcal{L}$ frame the debris satellite maintains a stationary position at the origin.

Figure 5.5 show a closer look at the local frame and how did the satellites approach their reference positions. We can divide this plot in rows and columns, where the first column shows the position for satellite s_1, the second column for satellite s_2, and the third column shows the position of satellite s_3 in the LVLH frame. The x, y and z axis in Figure 5.5 are the same axes as in Figure 5.3.

We see that the satellites approached a steady state at approximately 60 seconds. By manipulating weight Q and R in the objective function (5.4) we could decrease or increase the settling time, but we can assume that for our purpose it is equally important to approach the reference position as to reduce the fuel usage, thus we can set Q and R to be a diagonal matrix with values equal to one.

5.2.3 LQR performance considering J_2 effects

In this section analyzes the effects of J_2 disturbances on the performance of the controllers. Comparing Figures 5.3 and 5.6 we see that there is a slight effect on the motion of satellites due to the difference of J_2 between them. As they are relatively close to each other on the Earth's scale, the differential effect is low but noticeable. As in Figure 5.6 on the z axis the relative height is on scale of 10^{-4}.

It is also visible in Figure 5.8 on the z axis plots. Compare to Figure 5.5, where on the z axis there is no J_2 acceleration.

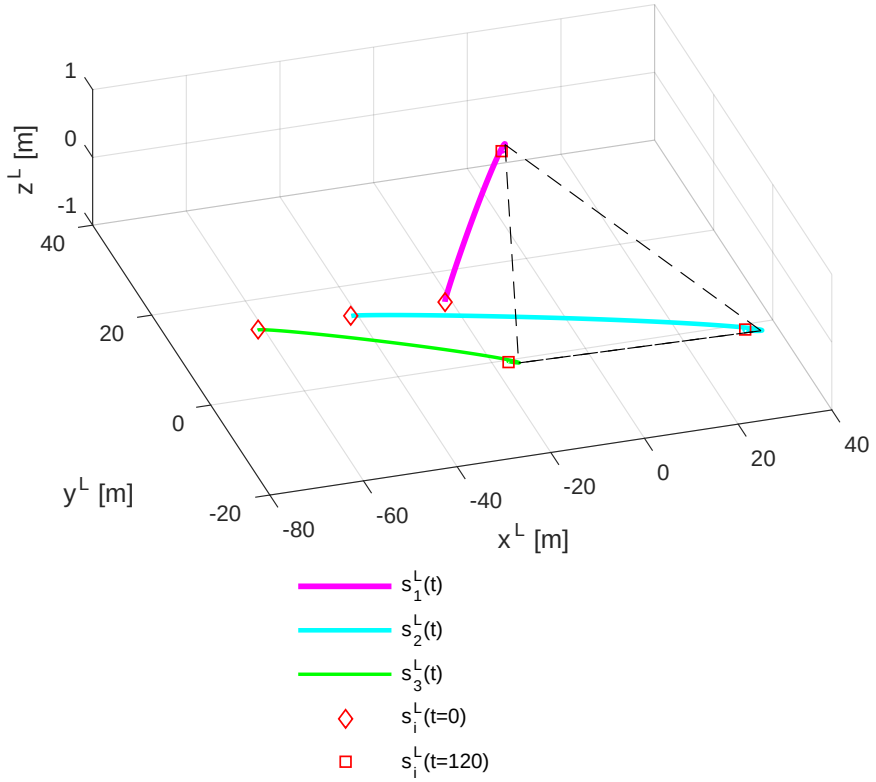

Figure 5.3: Satellite path with LQR controller in $\mathcal{L}$ frame without J_2 effect. Satellites initial position lies on x axis equal to -30, -50 -70 meters for s_1,s_2 and s_3 respectively.

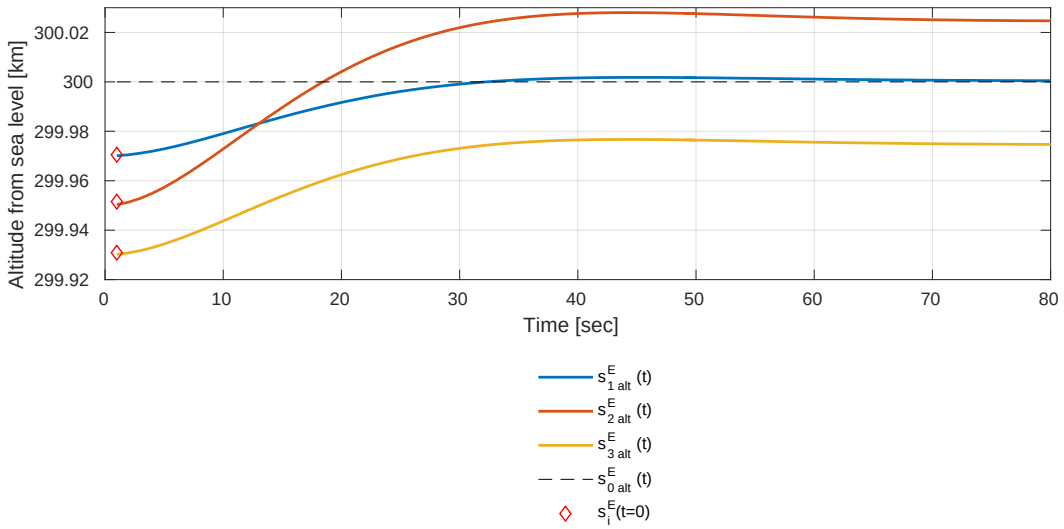

Figure 5.4: Satellites altitude change during simulation. The altitude in this graph is measured from the sea level excluding the J_2 effect. Initial altitude of $s^{\mathcal{E}}_{1alt}(t=0)$ is 299.97 [km] and 299.85[km], 299.83[km] altitude for $s^{\mathcal{E}}_{2alt}(t=0)$, $s^{\mathcal{E}}_{3alt}(t=0)$ respectively.$s^{\mathcal{E}}_{0alt}(t)$ is the altitude of the debris satellite with respect tot time.

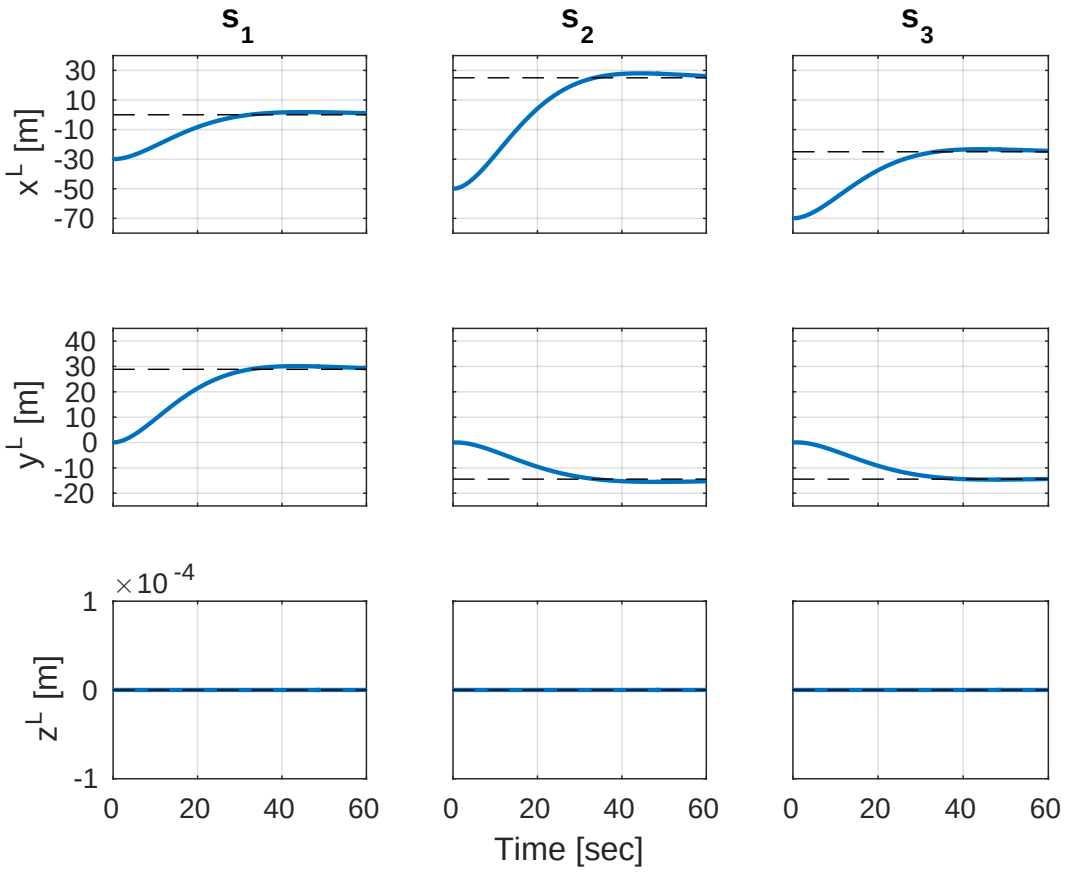

Figure 5.5: Satellites position on x, y and z coordinates with respect to time in the $\mathcal{L}$ frame. We notice that it takes approximately 60 seconds for satellites to reach steady state. As in this simulation we do not have the J_2 effect, satellites stay on the same z axis value as during the initial conditions, namely zero.

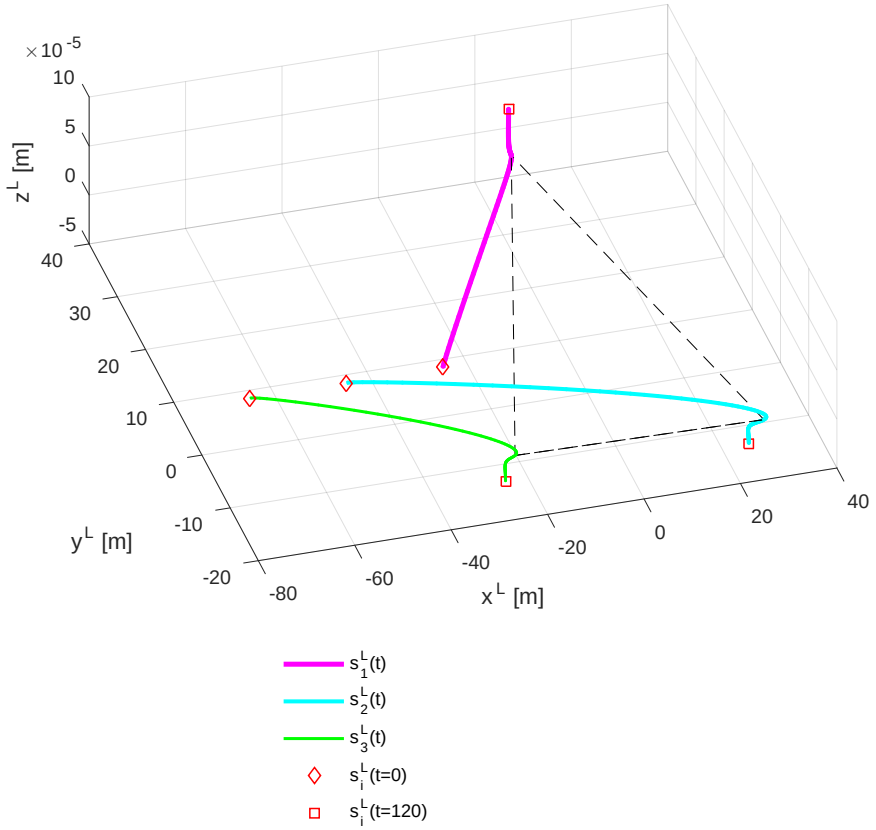

Figure 5.6: Satellite path with LQR controller in $\mathcal{L}$ frame with J_2 effect.s Satellites initial position lies on x axis equal to -30, -50 -70 meters for $s_1(t)$, $s_2(t)$ and $s_3(t)$ respectively.

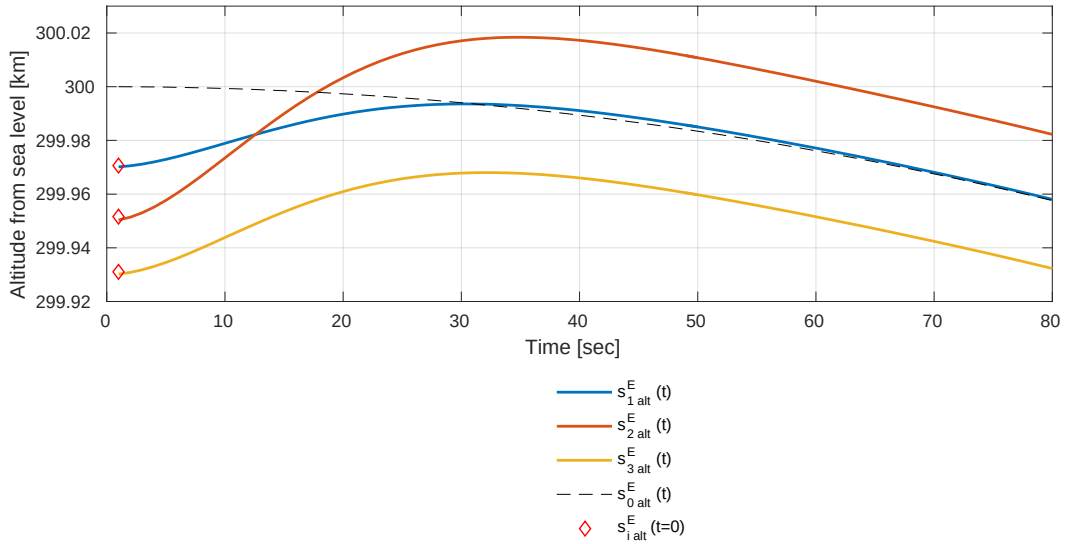

Figure 5.7: Satellites altitude change during simulation including the J_2 effect. The altitude in this graph is measured from the origin of the ECI frame excluding the J_2 effect. In this figure we see a decrease in altitude. This decrease in altitude is expected as we discussed in Chapter 3.1.2 and more particularly in Figure 3.3. Initial altitude of $s^{\mathcal{E}}_{1alt}(t=0)$ is 299.97 [km] and 299.85[km], 299.83[km] altitude for $s^{\mathcal{E}}_{2alt}(t=0)$, $s^{\mathcal{E}}_{3alt}(t=0)$ respectively.$s^{\mathcal{E}}_{0alt}(t)$ is the altitude of the debris satellite with respect tot time.

Figure 5.7 show an altitude plot in the Earth's frame, and we see that the effect is sufficiently big to be noticeable.

LQR simulation is important, because we can use it as our set point. We can compare other methods to it and establish the cost for maintaining formation. Intuitively the fuel cost should increase while maintaining formation on the way. The fuel is computed by saving the amount of force used and then multiplying it by a constant. In our case we use the I_{sp} value from Table 2. This value is in Newton seconds per kilogram, $[\frac{Ns}{kg}]$. In the simulation our time step is 1 second, and during this second we have a certain thrust due to control action. This means that we apply some force during a certain period of time which can be expressed in Newton seconds $[Ns]$. By multiplying force applied with its duration and by the inverse of the specific impulse value from Table 2 we get the total amount of fuel used during a certain action. We can see this clearly when multiplying units of these values, namely $[Ns\frac{kg}{Ns}] = [kg]$. During this simulation the following results for fuel consumption were obtained.

	No J2	*With J2*
Fuel usage [kg]	0.5965	0.5965

Table 5.1: Fuel usage of the LQR controller in (5.5): We compare the case where the $J2$ effect is included with the case where this effect is not accounted for.

At this point the LQR shows us what performance we should expect from an MPC without constrains. This will also help us finding appropriate prediction horizon discussed in the next chapter.

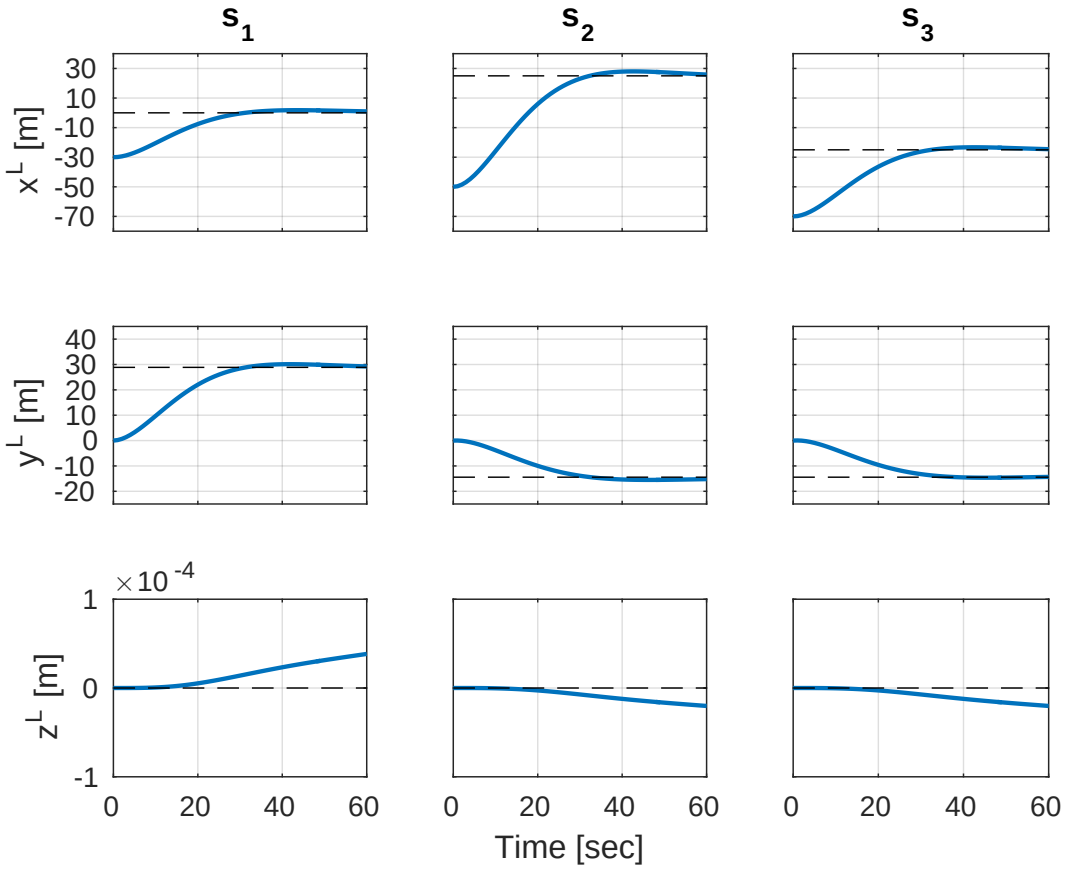

Figure 5.8: Satellites position on x, y and z coordinates with respect to time in the L frame including the J_2 effect. Figure shows the movement of each satellite in the Local-Horizontal, Local-Vertical frame. We notice that it takes approximately 60 seconds for satellites to reach steady state. With the J_2 effect, satellites have some relative J_2 acceleration that makes them lowly deviate from the initial conditions.

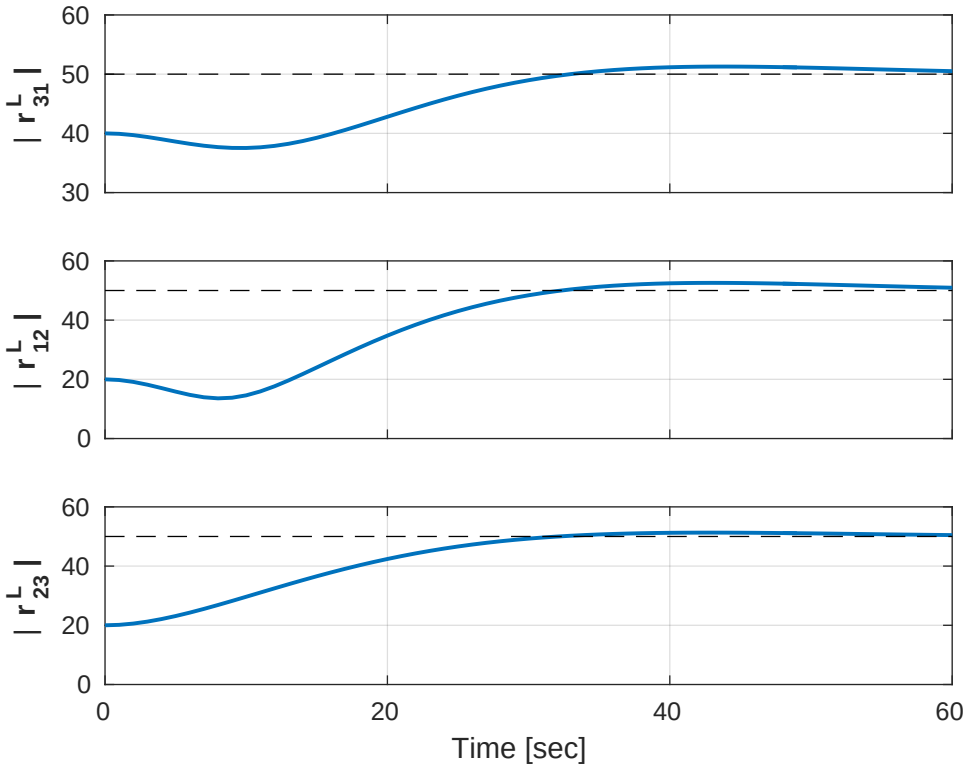

Figure 5.9: Distance between satellites with respect to time. The reference distance $\boldsymbol{r}_{ij}$ as set to 50 [m]. We see that the satellites only obtained formation when they approached the reference positions at the origin.

5.3 Model Predictive Control

MPC is an advanced method of process control with a finite prediction horizon. At each sampling time, MPC uses an estimate of the current state at time t and solves an optimal control problem for a system controlled in feed-forward. After solving the problem over the prediction horizon, MPC uses only the first value and sets it as an input to the system. At the next time step $t+1$ a new optimization problem needs to be solved with new states. This procedure is illustrated in Figure 5.10.

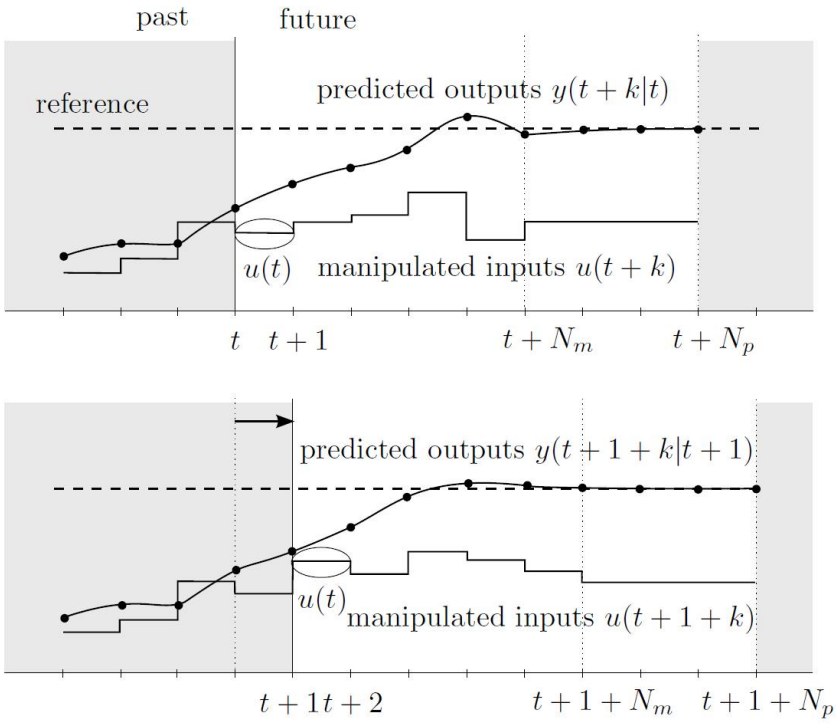

Figure 5.10: Scheme of how a Model predictive Control performs computations [7]. The MPC scheme solves the control problem for the current timeslot, while future timeslots are taken into account.

One of the biggest advantages of the MPC strategy is the ability to incorporate future disturbances / requirements where as LQR controllers do not have this predictive ability.

The initial step is finding a prediction horizon for MPC that will give similar results as LQR did in previous section. As we mentioned before, LQR is an optimal controller and MPC without any constrains should perform as good as LQR, thus indicating that the MPC set-up was correct. With the correct prediction horizon the satellites should manage to create formation at the origin as in LQR case. The biggest disadvantage with a large prediction horizon is that there is a larger chance for numerical error and the computational time increases rapidly. Our strategy will be to lower the prediction horizon, thus reducing the computational time, but still trying to maintain the performance of LQR. For solving a MPC problem we will use the YALMIP toolbox [12] combined with Matlab.

5.3.1 Formation at the origin versus following a path

We now propose and test the two methods mentioned in chapter 5.1, namely the formation at the origin and the following a predefined path with a center of formation. We start by stationary reference position $\boldsymbol{r}_i$ at the origin of the LVLH plane as illustrated in Figure 5.11. The objective function for this test is described by (5.2), with γ set to 1. Additionally we set constrains on input that is equal to $\boldsymbol{u}_{min} = 0[N]$ and $\boldsymbol{u}_{max} = 27[N]$. The simulation environment is as defined in Chapter 5.1.1. Figure 5.11 illustrates simulation done with the set-up mentioned above.

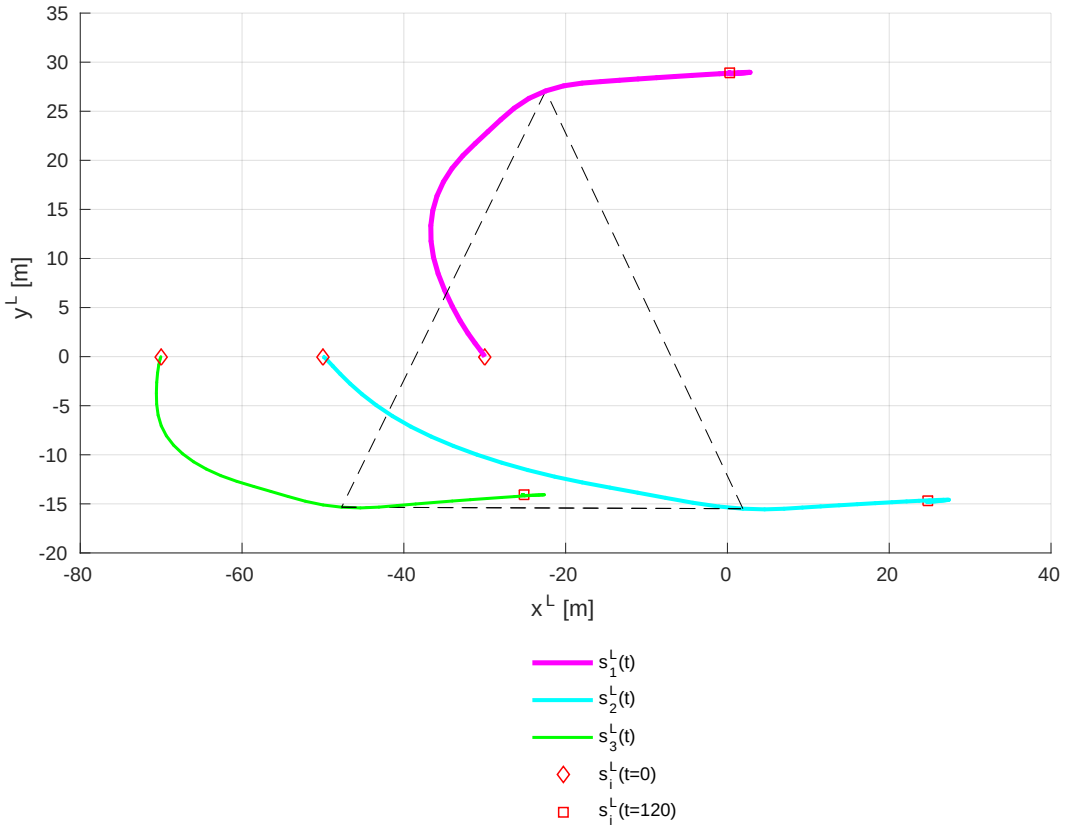

Figure 5.11: Satellites path with MPC by using problem description illustrated in Figure 5.11 in L frame with J_2 effect. Satellites initial position lies on x axis equal to -30, -50 -70 meters for s_1,s_2 and s_3 respectively.

The second method involves following a predefined path. This path was generated with by using a single satellite with an LQR controller. For this simulation we set the same initial conditions, same constants in objective function and same constrains as in simulation that is illustrated in Figure 5.11.

In both cases satellites obtain the formation almost simultaneously based on Figure 5.13. But the most interesting part is that the fuel consumption for satellites following a predefined path was less. This can be due to the low predictions horizon. During the simulation when following LQR path, we continuously update the reference position. So with a low prediction horizon might be enough to reach reference points that are close by but not enough to compute an optimal path for approaching the origin. We can increase the prediction horizon and see how

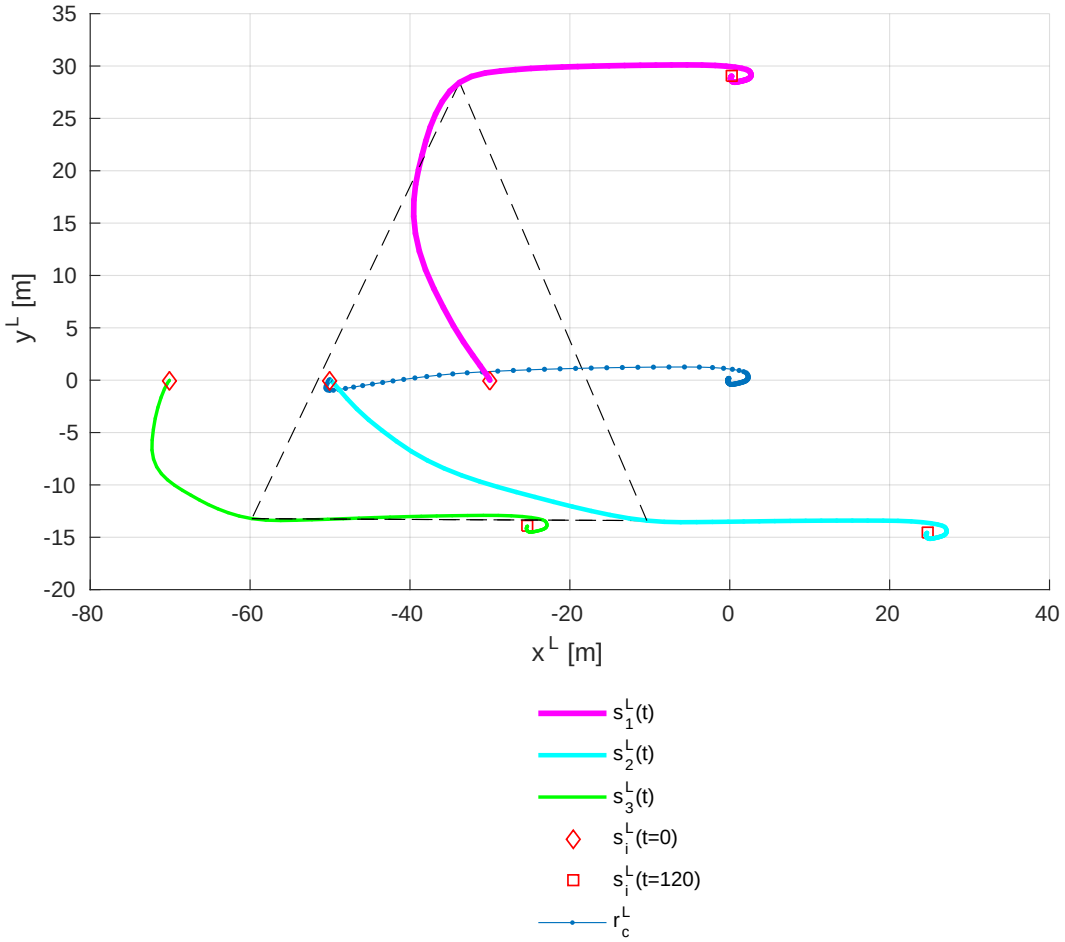

Figure 5.12: Satellites path with MPC by using problem description illustrated in Figure 5.12 in L frame with J_2 effect. Satellites initial position lies on x axis equal to -30, -50 -70 meters for s_1,s_2 and s_3 respectively.

does it effect the fuel consumption. All other constants that we defined in this section will stay the same.

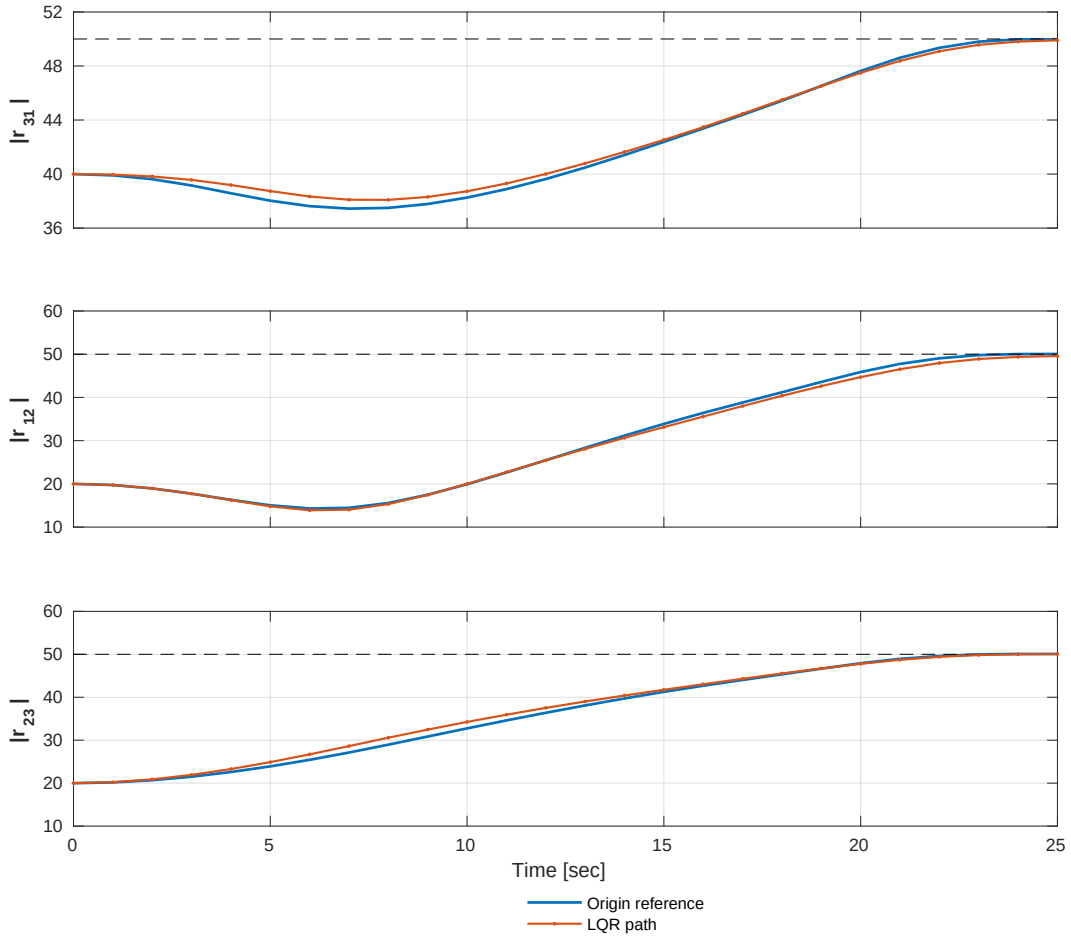

Figure 5.13: Relative distance between satellites with respect to time. $|r_{ij}|$ stands for the absolute distance between the satellites s_i and s_j in the local frame $\mathcal{L}$.

Figure 5.14 shows the result of this simulation. We see that by increasing the prediction horizon we can reduce the fuel consumption. But when we increase it above 35 seconds, we get some numerical errors. We also see when the prediction horizon is high enough, it becomes more efficient to use methods illustrated in Figure 5.1 than 5.2. To summarize, if the reference is relatively far, we can use an optimal predefined path. But if the prediction horizon is long enough to approach the reference position, then we can use the origin method.

5.3.2 Model predictive control with different weights in the cost function

In Chapter 5.1 we introduced the weight γ in the objective function (5.2). In this chapter we will compare the effects of selecting different weights in the control performance. The following Figure 5.15 compares $\gamma = 1$ and $\gamma = 5$. In the objective function, γ sets the relative importance

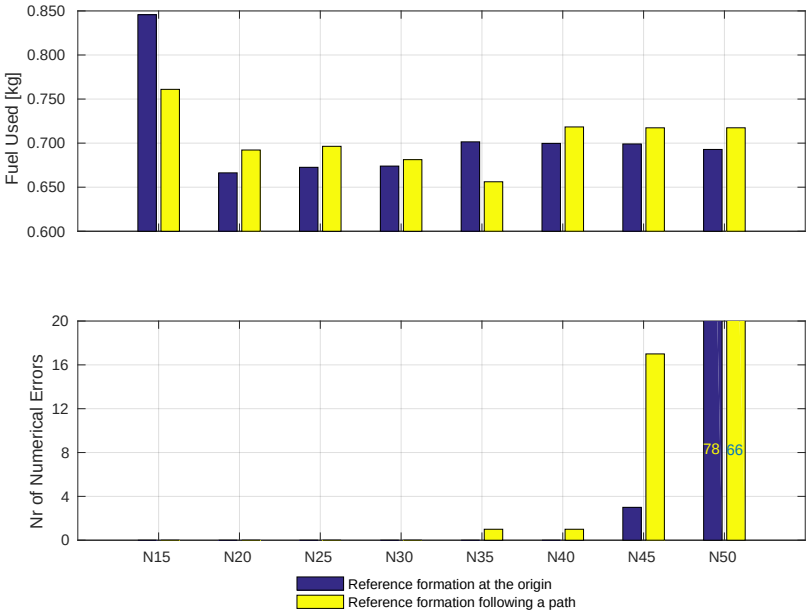

Figure 5.14: The total fuel consumption for 3 satellites in formation with respect to size of prediction horizon. The second graph shows the number of numerical problems YALMIP toolbox obtained during the simulation with respect to the size of the prediction horizon. The largest number of numerical errors during the simulation is 120.

on maintaining the formation versus maintaining the position.

We see that in Figure 5.15 the formation with $\gamma = 5$ obtains formation faster than the formation with $\gamma = 1$. The relative distance between satellites Figure 5.15 is plotted at the moment satellites have obtained formation. To know exactly when the satellites obtain formation, we can look at Figure 5.16. We can see it clearly when the satellites that had $\gamma = 5$ in the objective function obtained the formation at 17 seconds, where as formation with $\gamma = 1$ obtained it at time equal to 23 seconds. In other words we choose γ to set the importance of maintaining formation. So in case we would use them for Earth observation and maintaining formation would be important, we would set a higher γ.

The fuel used during this simulation for:

	$\gamma = 1$	$\gamma = 5$
Fuel usage [kg]	0.85	1.17

Table 5.2: Fuel usage of the MPC controller with objective function (5.2). Values in the table refer to Figure 5.15 and shows that if we choose to construct formation on before approaching reference position, it will result in a more costly maneuver. The additional fuel usage comes from the extra path that satellites takes during the formation construction.

This is due to the particular mission where our final destination are the reference points around the origin. When $\gamma = 5$ satellites travel extra path before reaching the final destination.

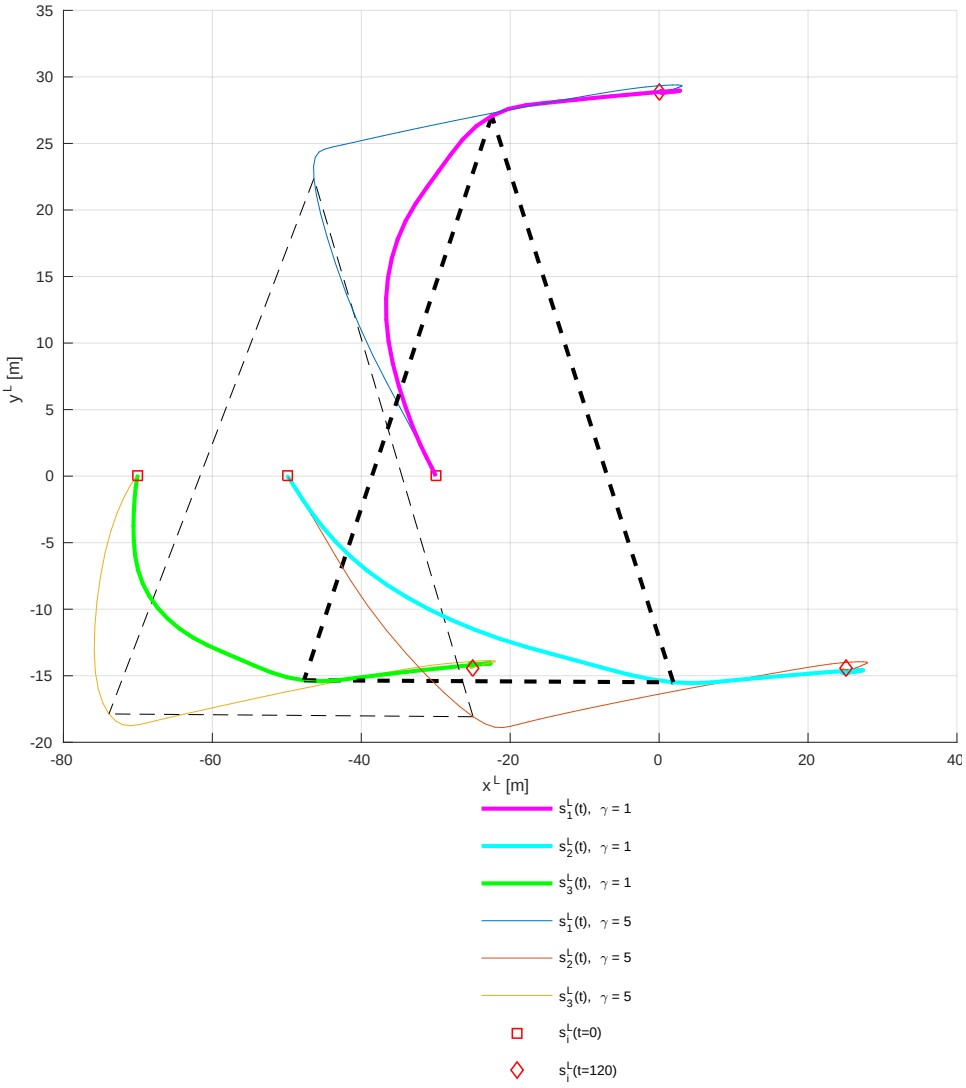

Figure 5.15: Comparison between satellites path with MPC by using problem description illustrated in Figure 5.11 in L frame with J_2 effect. Satellites initial position lies on x axis equal to -30, -50 -70 meters for s_1,s_2 and s_3 respectively. γ is weight put on maintaining formation.

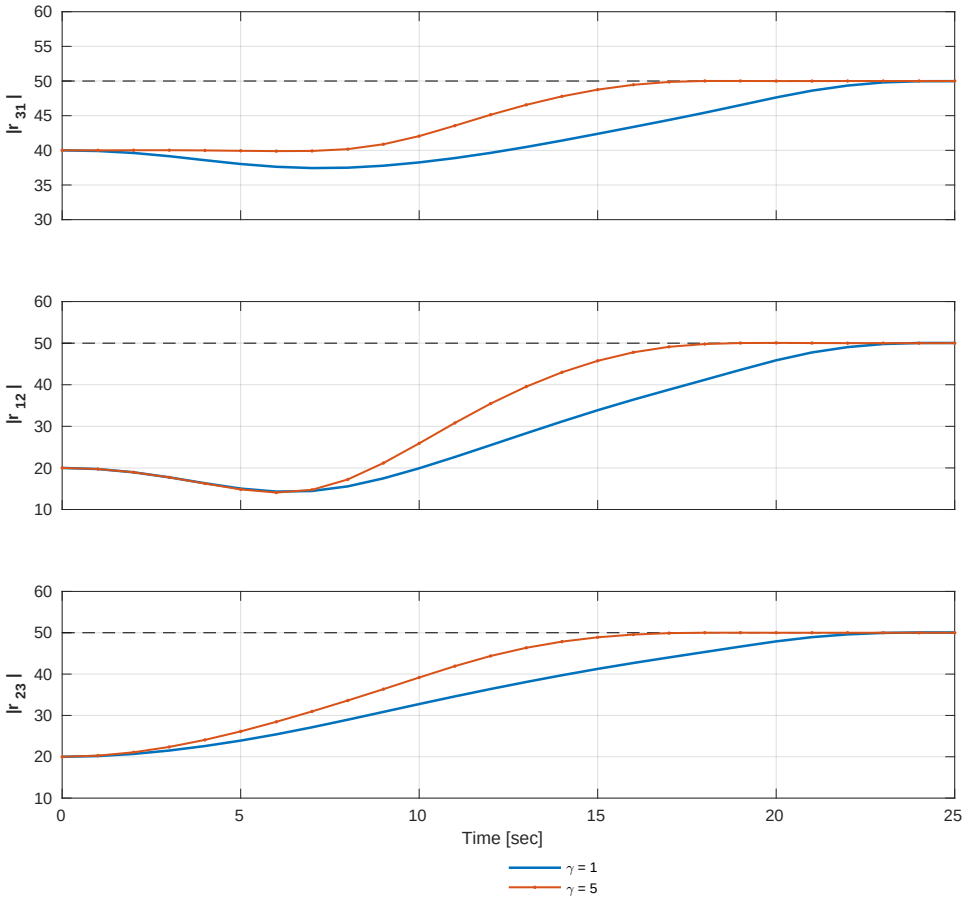

Figure 5.16: Relative distance between satellites with respect to time. $|r_{ij}|$ stands for the absolute distance between the satellites s_i and s_j.

5.3.3 Model predictive control with different State Space approaches

This chapter compares different constrains in the MPC formulation. In other words, we want to find out how much we could save on fuel by including the relative J_2 effect between the satellites inside the MPC. In this test we will start from the same initial conditions as before, but we will increase the distance between the satellites to increase the relative J_2 effect. The reference distance between the satellites will be 1 [km] and we will maintain this formation for 8 minutes. The simulation is shown in Figure 5.17.

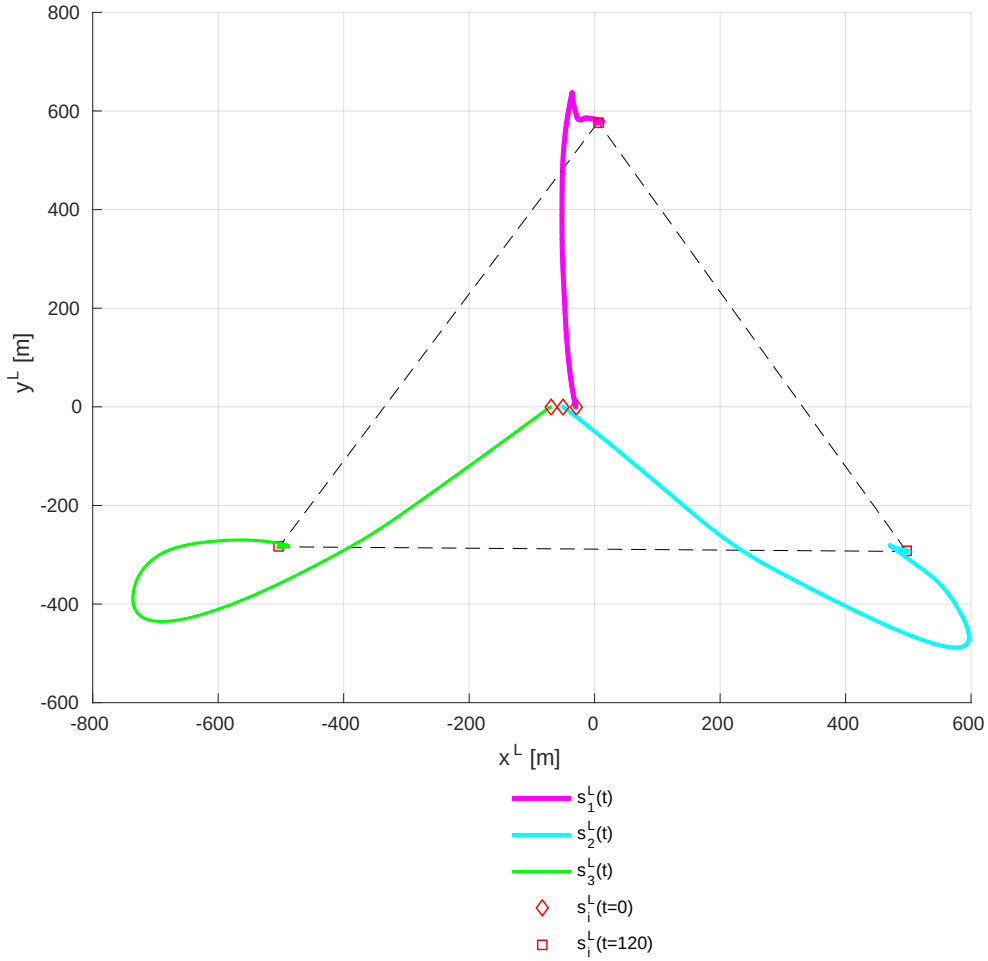

Figure 5.17: Representation of the simulation to test different strategies for minimizing fuel consumption. Satellites initial position lies on x axis equal to -30, -50 -70 meters for s_1,s_2 and s_3 respectively. To increase the relative J_2 effect between satellites, the reference distance between satellites has been set to be 1 [km].

Model A **:** This model was used in all previous examples and simulation, namely objective function described by (5.2). And where constrains were subjected to Clohessy-Wiltshire model. Model A will also be used as a reference model to compare if the modified methods can actually

increase performance.

$$\begin{aligned}
\text{minimize} \quad & \sum_{k=t}^{N} \left(\sum_{i=1}^{3} \left[||\boldsymbol{x}_i(k) - \boldsymbol{r}_i(k)||_Q^2 + ||\boldsymbol{u}_i(k)||_R^2 \right] + \gamma \sum_{j \neq i} ||(\boldsymbol{x}_i(k) - \boldsymbol{x}_j(k)) - \boldsymbol{r}_{ij}||_{Q'}^2 \right) \\
\text{subjected to:} \quad & \boldsymbol{x}_i^+ = A_d \boldsymbol{x_i} + B_d \boldsymbol{u_i} \quad i,j \in \{1...3\}, k = 0 \dots N \\
& \boldsymbol{x}_i = \begin{bmatrix} x_i & y_i & z_i & \dot{x}_i & \dot{y}_i & \dot{z}_i \end{bmatrix}^T, \\
& \boldsymbol{u}_i = \begin{bmatrix} u_{x_i^+} & u_{y_i^+} & u_{z_i^+} & u_{x_i^-} & u_{y_i^-} & u_{z_i^-} \end{bmatrix}^T
\end{aligned} \tag{5.6}$$

Model B **:** In this model we will modify the A with A_d^{J2} matrix in the constrains of MPC. A_d^{J2} matrix is based on model described in 4.15 in Chapter 4.2. The reason why this model should reduce the fuel consumption is due to the fact that this model includes the J_2 effect. In other words, the A_d^{J2} matrix has the information about the J_2 disturbance, so it should be able to make better predictions.

$$\begin{aligned}
\text{minimize} \quad & \sum_{k=t}^{N} \left(\sum_{i=1}^{3} \left[||\boldsymbol{x}_i(k) - \boldsymbol{r}_i(k)||_Q^2 + ||\boldsymbol{u}_i(k)||_R^2 \right] + \gamma \sum_{j \neq i} ||(\boldsymbol{x}_i(k) - \boldsymbol{x}_j(k)) - \boldsymbol{r}_{ij}||_{Q'}^2 \right) \\
\text{subjected to:} \quad & \boldsymbol{x}_i^+ = A_d^{J2} \boldsymbol{x_i} + B_d \boldsymbol{u_i} \quad i,j \in \{1...3\}, k = 0 \dots N \\
& \boldsymbol{x}_i = \begin{bmatrix} x_i & y_i & z_i & \dot{x}_i & \dot{y}_i & \dot{z}_i \end{bmatrix}^T, \\
& \boldsymbol{u}_i = \begin{bmatrix} u_{x_i^+} & u_{y_i^+} & u_{z_i^+} & u_{x_i^-} & u_{y_i^-} & u_{z_i^-} \end{bmatrix}^T
\end{aligned} \tag{5.7}$$

Model C **:** In this model we will use Model A and add an additional term inside the constrains on the assumption that based on the position in the $\mathcal{E}$ frame, we know the relative effect of the J_2 on satellites. This means that the A matrix will stay the same as in Model A.

$$\begin{aligned}
\text{minimize} \quad & \sum_{k=t}^{N} \left(\sum_{i=1}^{3} \left[||\boldsymbol{x}_i(k) - \boldsymbol{r}_i(k)||_Q^2 + ||\boldsymbol{u}_i(k)||_R^2 \right] + \gamma \sum_{j \neq i} ||(\boldsymbol{x}_i(k) - \boldsymbol{x}_j(k)) - \boldsymbol{r}_{ij}||_{Q'}^2 \right) \\
\text{subjected to:} \quad & \boldsymbol{x}_i^+ = A_d \boldsymbol{x_i} + B_d \boldsymbol{u_i} + \boldsymbol{F_i^{J2}} \quad i,j \in \{1...3\}, k = 0 \dots N \\
& \boldsymbol{x}_i = \begin{bmatrix} x_i & y_i & z_i & \dot{x}_i & \dot{y}_i & \dot{z}_i \end{bmatrix}^T, \\
& \boldsymbol{u}_i = \begin{bmatrix} u_{x_i^+} & u_{y_i^+} & u_{z_i^+} & u_{x_i^-} & u_{y_i^-} & u_{z_i^-} \end{bmatrix}^T
\end{aligned} \tag{5.8}$$

Results **:** During this simulation Model A consumed 6.22 kilograms of propellant, where as Model B and Model C only 6.048 kilograms. This result is summarized in Figure 5.18. The reason why Model B and Model C perform identically is that in both cases J_2 is included and the only difference is that either we include it in an A matrix or as an additional term. In case of LQR, same procedure could not be possible and we would have to use A_d^{J2} matrix to reduce the cost.

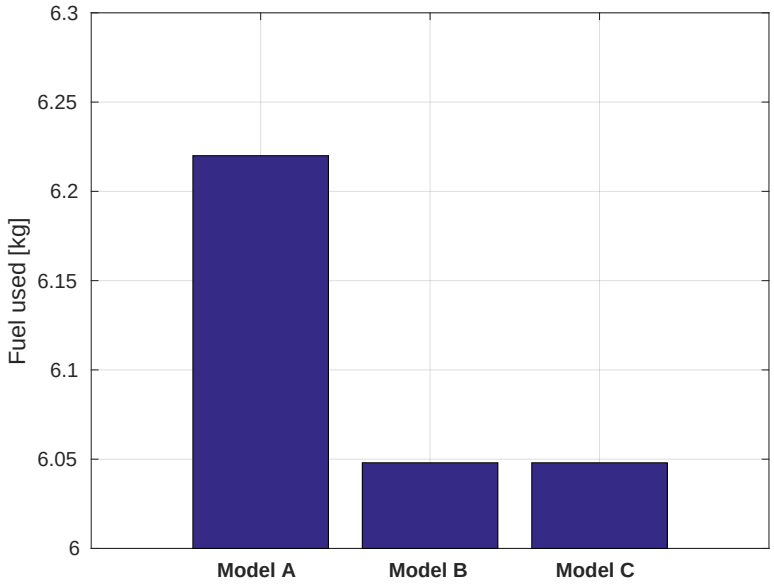

Figure 5.18: Fuel consumption results. We see that by including the J_2 effect in the MPC it is possible to reduce the amount of propellant used.

Chapter 6

Stochastic Model Predictive Control

This chapter is dedicated to the case when the model parameters have some known uncertainty. For example, in our case we can assume that the bi-propellant thrusters of the various satellites have an uncertain thrust output, namely if the controller sets an output of $1[N]$ the thruster might instead provide an output of $0.9[N]$ or $1.1[N]$. We will assume that our uncertainty is normally distributed [1].

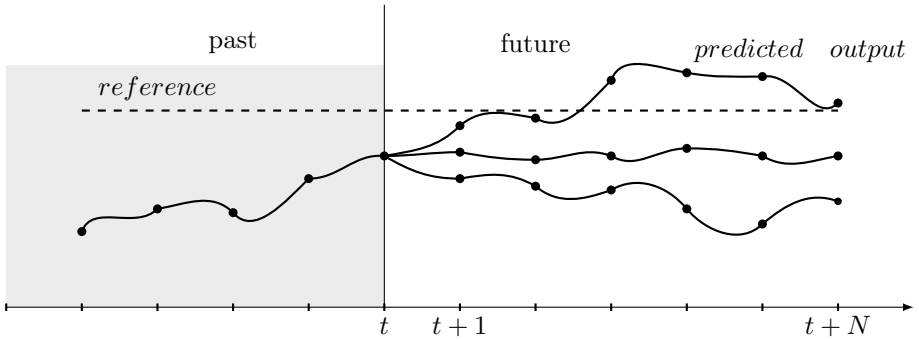

Figure 6.1: MPC with thrust uncertainty. We see that if we do not include any information into the MPC about the possible disturbance, the output might vary more than expected, thus making it a suboptimal solution.

We will counteract this uncertainty by a known technique that corresponds to including additional constrains to the MPC, thus providing more information about the dynamic environment. If we compare Figure 6.1 with Figure 6.2 we see that on average the performance of Figure 6.2 will be higher, and this is the performance that we expect by adding additional constraints to the MPC. The downside of this technique, called Stochastic Model Predictive Control (SMPC), is that by adding more constraints, the problem becomes more numerically difficult to solve; thus we expect that by applying this technique it will take more computational time for estimating an optimal output.

[1] The motivation is inspired by the central limit theorem [10], that says that under general conditions the sum of a large number of independent factors results in an approximately normally distributed total effect.

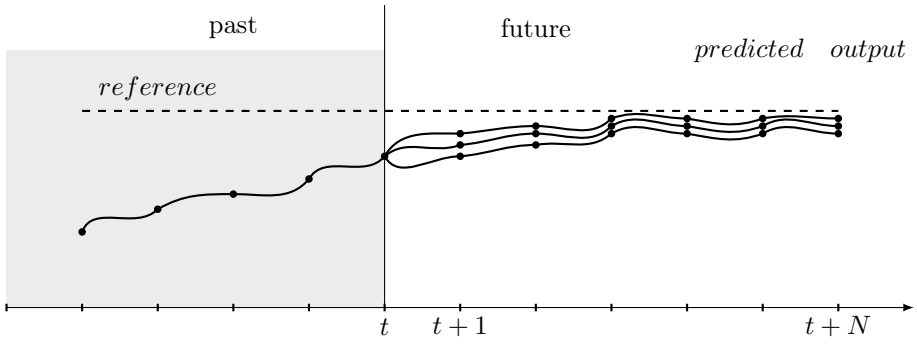

Figure 6.2: SMPC with thrust uncertainty. By including information about the range of possible uncertainty, the performance of SMPC increases.

6.1 Control problem formulation

For our problem with uncertainties, the objective function is represented in (6.1). The main difference between (6.1) and the MPC's objective functions is that we add additional constrains.

$$
\begin{aligned}
\text{minimize} \quad & \sum_{k=t}^{N} \left(\sum_{i=1}^{3} \left[||\boldsymbol{x}_i(k) - \boldsymbol{r}_i(k)||_Q^2 + ||\boldsymbol{u}_i(k)||_R^2 \right] + \gamma \sum_{j \neq i} ||(\boldsymbol{x}_i(k) - \boldsymbol{x}_j(k)) - \boldsymbol{r}_{ij}||_{Q'}^2 \right) \\
\text{subjected to:} \quad & \boldsymbol{x}_i^+ = A_d \boldsymbol{x_i} + B_d \boldsymbol{u}_i + \boldsymbol{F}_i^{J2} + \boldsymbol{e}_1 \quad i, j \in \{1...3\}, k = 0 \dots N \\
& \boldsymbol{x}_i^+ = A_d \boldsymbol{x_i} + B_d \boldsymbol{u}_i + \boldsymbol{F}_i^{J2} + \boldsymbol{e}_2 \\
& \vdots \\
& \boldsymbol{x}_i = \begin{bmatrix} x_i & y_i & z_i & \dot{x}_i & \dot{y}_i & \dot{z}_i \end{bmatrix}^T, \\
& \boldsymbol{u}_i = \begin{bmatrix} u_{x_i^+} & u_{y_i^+} & u_{z_i^+} & u_{x_i^-} & u_{y_i^-} & u_{z_i^-} \end{bmatrix}^T
\end{aligned}
\tag{6.1}
$$

By doing so, we actually provide the possible scenarios that might happen. In general we would like to avoid adding more constrains, but in this case this makes the MPC more robust to uncertainties. In words, thus, we generate scenarios by randomly generating uncertainty and adding it to the state space model.

6.2 Model Predictive control with thrust uncertainty

Simulations are done by varying the standard deviation on the uncertainty on the propellers σ and on the number of scenarios that will be generated so to account for this uncertainty. More specifically the number of scenarios is the number of e_i's generated in (6.1), and it will provide information about the number of constrains that were added to the original MPC formulation. We start considering $\sigma = 1$ in a simulation that is done by generating a random noise with normal distribution and then reusing the same noise for every simulation while varying the number of scenarios. The SMPC has no information about the true noise that affect the satellites, but have a credible information on the distribution of this noise. In Figure 6.3 we see that using more scenarios leads to a decrease in the fuel consumption. It can nonetheless happen that we

actually use more fuel with increasing the numbers of scenarios, as in Figure 6.3 when we compare using 10 and using 20 scenarios. This implies that we can not guarantee that by including more scenarios we will reduce the fuel cost. But we can say that, on average (as it will be shown in Figure 6.5), the more scenarios we add the less fuel will be used and the more robust the system will be with respect to uncertainties.

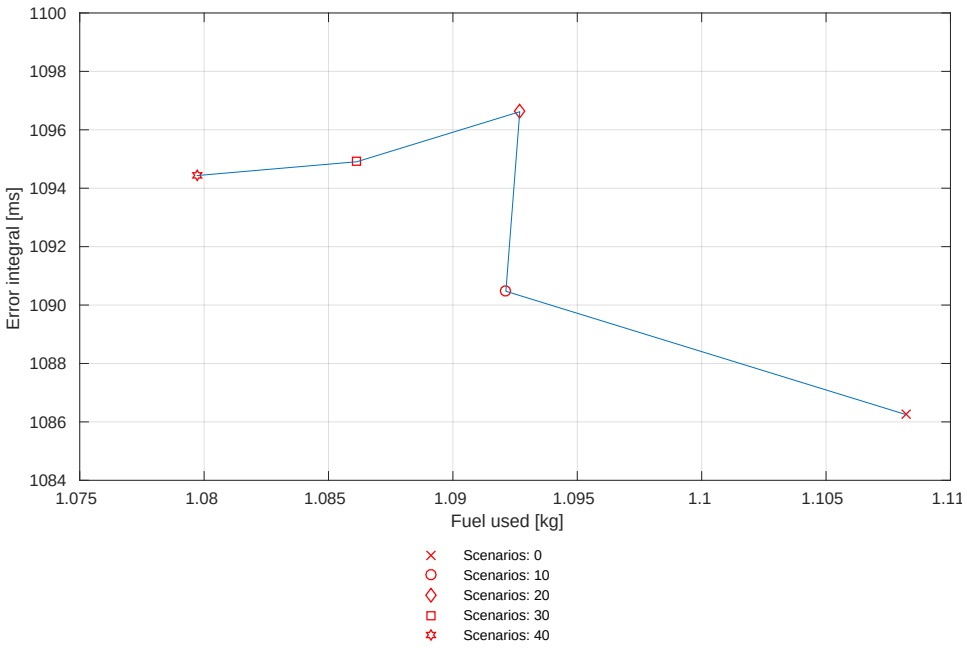

Figure 6.3: Comparison between the two performance indexes with variance $\sigma = 1$. Fuel used stand for the total amount of fuel used by 3 satellites during a 120 second simulation. Error integral is a stepwise multiplication between the reference position and the actual position of a satellites and the time period.

We now consider the case where the uncertainty level on the thrusters is equal to $\sigma = 3$. As we see in Figure 6.4 this leads to the same effect on the satellites as in the case $\sigma = 1$. The only difference is that as we include more variance, the satellites stay away from the desired position longer. This problem could be solve by including larger number on scenarios, but this would increase the computational time rapidly, so with large amount of scenarios SMPC might not have enough time to compute an optimal input when it is needed. So if we choose to use SMPC techniques we should choose the amount of scenarios based on the computational power that we have. We can do an attentional test with new noise but lower number of constraints and show that on average we can expect that the fuel consumption will decrease as we add more scenarios. In Figure 6.5 we plot the average between our performance indexes.

With these preliminary results we have shown that Stochastic Model Predictive Control is a good candidate for counteracting disturbances such as thrust uncertainty. As the uncertainty was added to constrains as an additional term, same procedure can be used to add drag force and solar wind acting on the spacecraft in low Earth's orbit.

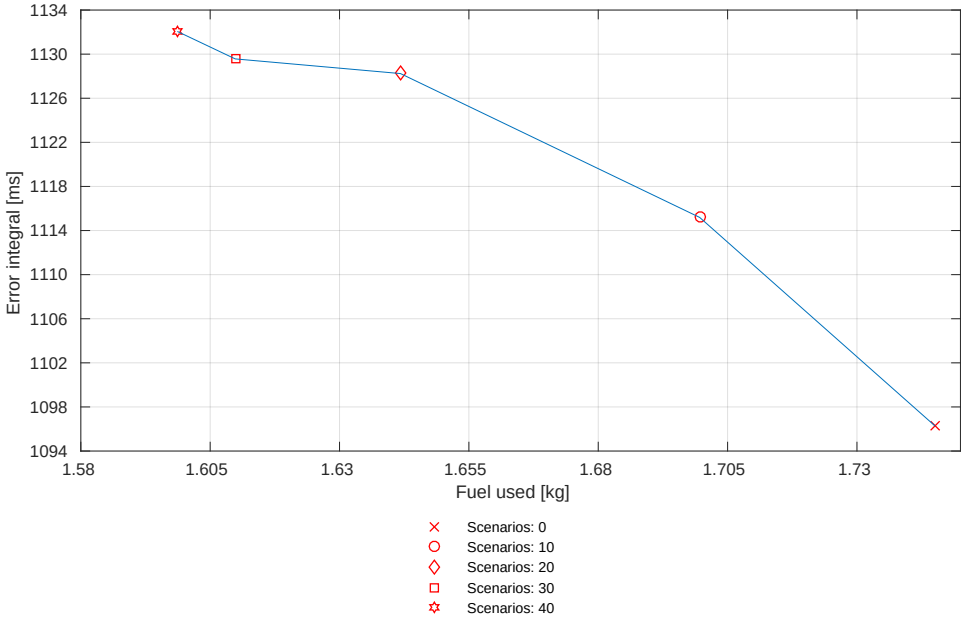

Figure 6.4: Comparison between to performance indexes with variance $\sigma = 3$. Fuel used stand for the total amount of fuel used by 3 satellites during a 120 second simulation. Error integral is a stepwise multiplication between the reference position and the actual position of a satellites and the time period.

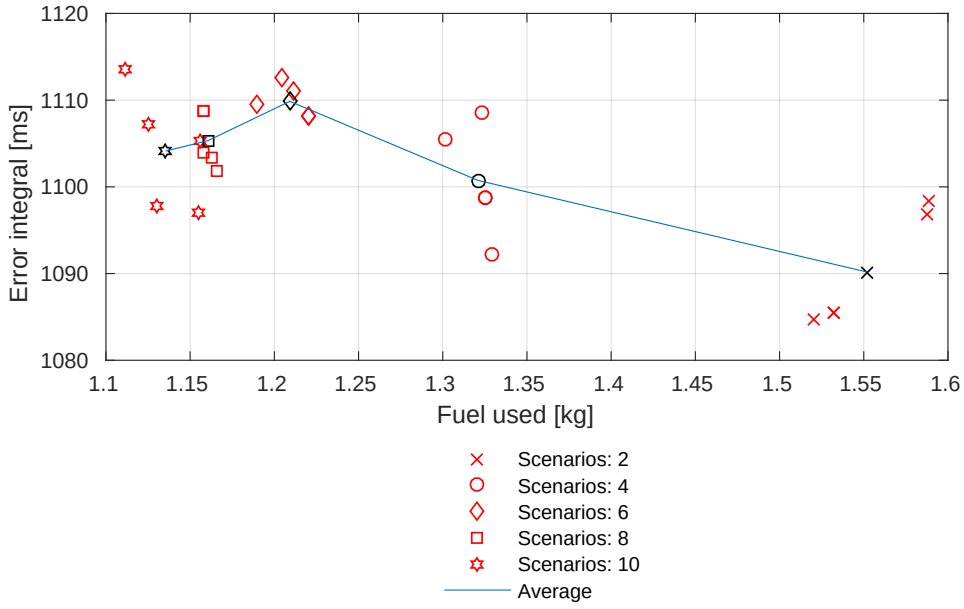

Figure 6.5: Comparison between to performance indexes with variance $\sigma = 1$. Fuel used stand for the total amount of fuel used by 3 satellites during a 120 second simulation. Error integral is a stepwise multiplication between the reference position and the actual position of a satellites and the time period. The blue line indicates an average trend of two performance indexes.

Chapter 7

Conclusions and Future work

We have shown that model predictive control is a suitable method for controlling a fleet of satellites, and also shown that by modifying the MPC formulation to include the J_2 effect we can achieve lower fuel consumption. Decrease in fuel usage can also be achieved by adjusting prediction horizon for the MPC. Our simulations have shown that by choosing different methods, such as following a predefined path, a reduction in fuel consumption can be achieved. In case of thrust input uncertainty, we have shown that lower fuel consumption can be achieved by selecting an appropriate amount of scenarios for the stochastic model predictive control.

Future work can include adding more disturbances such as the drag force or the solar wind. These disturbances can be measured or predicted, thus it is possible to add them to the MPC as we did with the relative J_2 effect. Additionally these disturbances will have some uncertainty, thus a SMPC can be used to counteract them as we did in case of thrust uncertainty. Additionally we can also include the attitude control for satellites. This means that we would need a control algorithm that adjusts the satellite S frame to desired angle. For this purpose we could use rotational matrices to transform between $\mathcal{L}$ frame and S. Additional constrains can be added by assuming that the relative distance between satellites can only be measured at a certain attitude range.

Appendix A

Background material

In this appendix we collect a few prerequisite notions on the physical modeling of orbital dynamics and a brief definition of the optimal infinite horizon problem known as LQR.

A.1 Equations of motion in a rotating frame

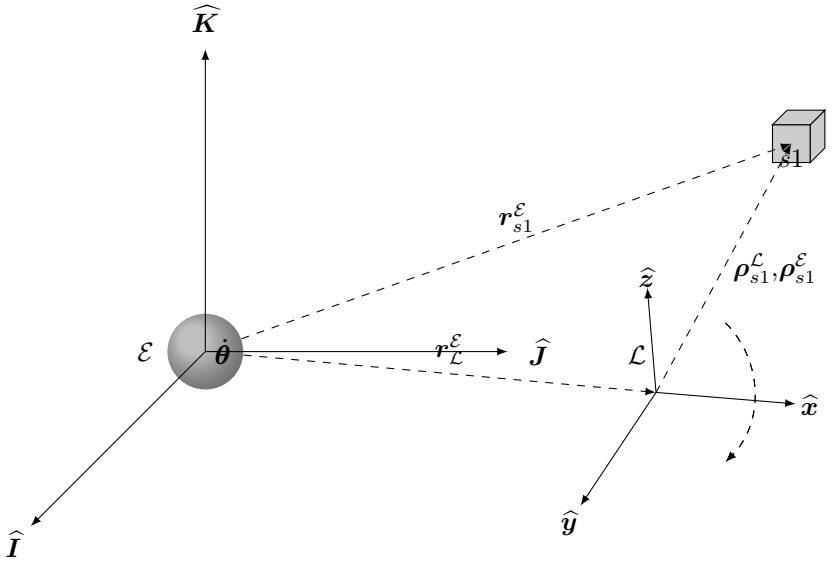

Figure A.1: Graphical representation of the ECI ($\mathcal{E}$) , LVLH ($\mathcal{L}_i$) and satellites frame ($\mathcal{S}_i$). Satellites frame ($\mathcal{S}_i$) lies on the LVLH frame ($\mathcal{L}_i$) and has the same origin. For formation control, we will consider that frame ($\mathcal{S}_i$) follows ($\mathcal{L}_i$) and has identical position and attitude.

Assume that the available measurement systems return information on the quantities $\boldsymbol{r}^{\mathcal{E}}_{\mathcal{L}}$, $\boldsymbol{r}^{\mathcal{E}}_{1}$, $\boldsymbol{\rho}^{\mathcal{L}}_{1}$, $\boldsymbol{\theta}$, $\dot{\boldsymbol{r}}^{\mathcal{E}}_{1}$ and $\dot{\boldsymbol{\theta}}$, so that we can assume them to be known. The task of this section is to compute the quantity

$$\ddot{\boldsymbol{\rho}}^{\mathcal{L}}_{1} = \phi\left(\boldsymbol{r}^{\mathcal{E}}_{\mathcal{L}}, \boldsymbol{r}^{\mathcal{E}}_{1}, \boldsymbol{\rho}^{\mathcal{L}}_{1}, \dot{\boldsymbol{\theta}}\right). \tag{A.1}$$

The derivation is as follows: consider the auxiliary variable $\boldsymbol{\rho}_1^{\mathcal{E}} := \boldsymbol{r}_{\mathcal{L}}^{\mathcal{E}} - \boldsymbol{r}_1^{\mathcal{E}}$ so that

$$\boldsymbol{r}_1^{\mathcal{E}} = \boldsymbol{r}_{\mathcal{L}}^{\mathcal{E}} + \boldsymbol{\rho}_1^{\mathcal{E}} \tag{A.2}$$

that imply immediately

$$\dot{\boldsymbol{r}}_1^{\mathcal{E}} = \dot{\boldsymbol{r}}_{\mathcal{L}}^{\mathcal{E}} + \dot{\boldsymbol{\rho}}_1^{\mathcal{E}} \tag{A.3}$$

and

$$\ddot{\boldsymbol{r}}_1^{\mathcal{E}} = \ddot{\boldsymbol{r}}_{\mathcal{L}}^{\mathcal{E}} + \ddot{\boldsymbol{\rho}}_1^{\mathcal{E}} \tag{A.4}$$

To simplify the calculations one can start by doing the derivation in $\widehat{\boldsymbol{I}}, \widehat{\boldsymbol{J}}$ plane. Assuming that a satellite orbits around equator, thus making $\widehat{\boldsymbol{K}}$ components equal to zero. This assumption is represented in figure A.2. Consider that LVLH plane has an angular velocity $\dot{\boldsymbol{\theta}}$ and is rotating around $\widehat{\boldsymbol{z}}$ axis. Thus, $\dot{\boldsymbol{\theta}} = \begin{bmatrix} 0 & 0 & \dot{\theta} \end{bmatrix}^T$. Assuming that at time $t = 0$ both frames are aligned, $\boldsymbol{\rho}_1^{\mathcal{E}}$

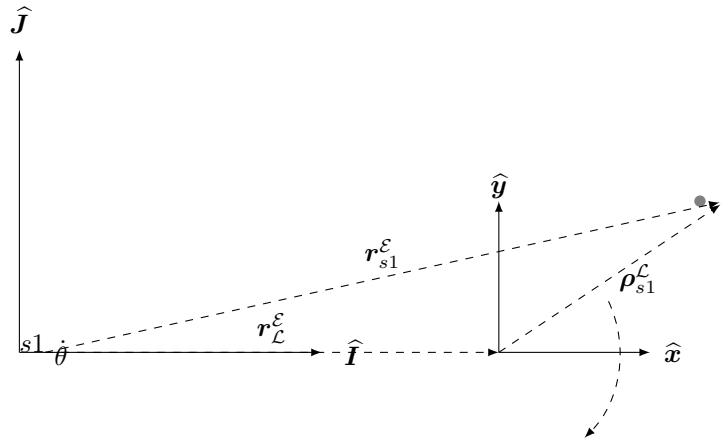

Figure A.2: Graphical representation of the ECI and LVLH frames considered in $\widehat{\boldsymbol{I}}$ and $\widehat{\boldsymbol{J}}$ coordinate frame.

can be expressed with help of a local frame

$$\boldsymbol{\rho}_1^{\mathcal{E}} = \left[\rho_1^{\mathcal{L}} \cos(\theta)\widehat{\boldsymbol{x}} + \rho_1^{\mathcal{L}} \sin(\theta)\widehat{\boldsymbol{y}}\right] \tag{A.5}$$

θ can be replaced with $\dot{\theta}t$ with assumption that both frames are aligned at $t = 0$. We are doing this step to be able to derivative our equation with respect to time.

$$\boldsymbol{\rho}_1^{\mathcal{E}} = \left[\rho_1^{\mathcal{L}} \cos(\dot{\theta}t)\widehat{\boldsymbol{x}} + \rho_1^{\mathcal{L}} \sin(\dot{\theta}t)\widehat{\boldsymbol{y}}\right] \tag{A.6}$$

Thus its derivative with respect to time is

$$\frac{d}{dt}\boldsymbol{\rho}_1^{\mathcal{E}} = \frac{d\rho_1^{\mathcal{L}}}{dt}\left[\cos(\dot{\theta}t)\widehat{\boldsymbol{x}} + \sin(\dot{\theta}t)\widehat{\boldsymbol{y}}\right] + \dot{\theta}\left[-\rho_1^{\mathcal{L}} \sin(\dot{\theta}t)\widehat{\boldsymbol{x}} + \rho_1^{\mathcal{L}} \cos(\dot{\theta}t)\widehat{\boldsymbol{y}}\right]. \tag{A.7}$$

Letting

$$\frac{d}{dt}\boldsymbol{\rho}_1^{\mathcal{L}} \doteq \frac{d\rho_1^{\mathcal{L}}}{dt}\left[\cos\left(\dot{\theta}t\right)\widehat{\boldsymbol{x}} + \sin\left(\dot{\theta}t\right)\widehat{\boldsymbol{y}}\right]$$

and

$$\dot{\boldsymbol{\theta}} \times \boldsymbol{\rho}_1^{\mathcal{L}} \doteq \dot{\theta}\left[-\rho_1^{\mathcal{L}} \sin(\dot{\theta}t)\widehat{\boldsymbol{x}} + \rho_1^{\mathcal{L}} \cos(\dot{\theta}t)\widehat{\boldsymbol{y}}\right]$$

we can rewrite (A.7) in compact form as[1]

$$\frac{d}{dt}\boldsymbol{\rho}_1^{\mathcal{E}} = \frac{d}{dt}\boldsymbol{\rho}_1^{\mathcal{L}} + \dot{\boldsymbol{\theta}} \times \boldsymbol{\rho}_1^{\mathcal{L}}. \tag{A.9}$$

By substituting Equation (A.9) into equation (A.3) velocity vector expression in the Earths frame is obtained

$$\dot{\boldsymbol{r}}_1^{\mathcal{E}} = \dot{\boldsymbol{r}}_{\mathcal{L}}^{\mathcal{E}} + \frac{d}{dt}\boldsymbol{\rho}_1^{\mathcal{L}} + \dot{\boldsymbol{\theta}} \times \boldsymbol{\rho}_1^{\mathcal{E}}. \tag{A.10}$$

The main objective here is to obtain accelerations that are affecting the motion of the satellite. Acceleration is derived by substituting equation (A.9) into (A.8). This means that we obtain

$$\begin{aligned}
\frac{d^2}{dt^2}\boldsymbol{\rho}_1^{\mathcal{E}} &\doteq \frac{d}{dt}\left(\frac{d}{dt}\boldsymbol{\rho}_1^{\mathcal{E}}\right) \\
&= \frac{d}{dt}\left(\frac{d}{dt}(\boldsymbol{\rho}_1^{\mathcal{L}}) + \dot{\boldsymbol{\theta}} \times \frac{d}{dt}(\boldsymbol{\rho}_1^{\mathcal{L}})\right) \\
&= \frac{d}{dt}\left(\frac{d}{dt}(\boldsymbol{\rho}_1^{\mathcal{L}}) + \dot{\boldsymbol{\theta}} \times \boldsymbol{\rho}_1^{\mathcal{L}}\right) + \dot{\boldsymbol{\theta}} \times \left(\frac{d}{dt}(\boldsymbol{\rho}_1^{\mathcal{L}}) + \dot{\boldsymbol{\theta}} \times \boldsymbol{\rho}_1^{\mathcal{L}}\right)
\end{aligned} \tag{A.11}$$

Since

$$\frac{d}{dt}\left(\frac{d}{dt}\boldsymbol{\rho}_1^{\mathcal{L}} + \dot{\boldsymbol{\theta}} \times \boldsymbol{\rho}_1^{\mathcal{L}}\right) = \frac{d^2}{dt^2}\boldsymbol{\rho}_1^{\mathcal{L}} + \frac{d}{dt}\left(\dot{\boldsymbol{\theta}} \times \boldsymbol{\rho}_1^{\mathcal{L}}\right) = \frac{d^2}{dt^2}\boldsymbol{\rho}_1^{\mathcal{L}} + \frac{d}{dt}\dot{\boldsymbol{\theta}} \times \boldsymbol{\rho}_1^{\mathcal{L}} + \dot{\boldsymbol{\theta}} \times \frac{d}{dt}\boldsymbol{\rho}_1^{\mathcal{L}} \tag{A.12}$$

and

$$\dot{\boldsymbol{\theta}} \times \left(\frac{d}{dt}\boldsymbol{\rho}_1^{\mathcal{L}} + \dot{\boldsymbol{\theta}} \times \boldsymbol{\rho}_1^{\mathcal{L}}\right) = \dot{\boldsymbol{\theta}} \times \frac{d}{dt}\boldsymbol{\rho}_1^{\mathcal{L}} + \dot{\boldsymbol{\theta}} \times \left(\dot{\boldsymbol{\theta}} \times \boldsymbol{\rho}_1^{\mathcal{L}}\right) \tag{A.13}$$

By substitution (A.12) ,(A.13) into (A.11) we obtain the relative acceleration expressed as a function of

$$\ddot{\boldsymbol{\rho}}_1^{\mathcal{E}} = \phi\left(\boldsymbol{\rho}_1^{\mathcal{L}}, \dot{\boldsymbol{\rho}}_1^{\mathcal{L}},\right). \tag{A.14}$$

$$\frac{d^2}{dt^2}\boldsymbol{\rho}_1^{\mathcal{E}} = \frac{d^2}{dt^2}\boldsymbol{\rho}_1^{\mathcal{L}} + 2\left(\dot{\boldsymbol{\theta}} \times \frac{d}{dt}\boldsymbol{\rho}_1^{\mathcal{L}}\right) + \frac{d}{dt}\dot{\boldsymbol{\theta}} \times \boldsymbol{\rho}_1^{\mathcal{L}} + \dot{\boldsymbol{\theta}} \times \left(\dot{\boldsymbol{\theta}} \times \boldsymbol{\rho}_1^{\mathcal{L}}\right). \tag{A.15}$$

where

- $2(\dot{\boldsymbol{\theta}} \times \frac{d}{dt}\boldsymbol{\rho}_1^{\mathcal{L}})$ - Coriolis acceleration
- $\frac{d}{dt}\dot{\boldsymbol{\theta}} \times \boldsymbol{\rho}_1^{\mathcal{L}}$ - Euler acceleration
- $\dot{\boldsymbol{\theta}} \times (\dot{\boldsymbol{\theta}} \times \boldsymbol{\rho}_1^{\mathcal{L}})$ - Centripetal acceleration

[1] Generalized version of equation (A.9) can be represented as

$$\frac{d\,(*)^{\mathcal{E}}}{dt} = \frac{d\,(*)_1^{\mathcal{L}}}{dt} + \dot{\boldsymbol{\theta}} \times (*)_1^{\mathcal{L}} \tag{A.8}$$

where $*$ can be any variable.

A.2 Transformation from Earth's frame to local-vertical, local-horizontal frame

As we have well defined local frame, the transformation from $\mathcal{E}$ to $\mathcal{L}$ can be done with few following matrix operations.

$$x^{\mathcal{L}} = \frac{r^{\mathcal{E}}}{|r^{\mathcal{E}}|} \tag{A.16}$$

$$y^{\mathcal{L}} = \frac{v^{\mathcal{E}}}{|v^{\mathcal{E}}|} \tag{A.17}$$

$$z^{\mathcal{L}} = \frac{x^{\mathcal{L}} \times y^{\mathcal{L}}}{|x^{\mathcal{L}} \times y^{\mathcal{L}}|} \tag{A.18}$$

$$R^{\mathcal{E}}_{\mathcal{L}} = \begin{bmatrix} x^{\mathcal{L}} & y^{\mathcal{L}} & z^{\mathcal{L}} \end{bmatrix} \tag{A.19}$$

$$R^{\mathcal{L}}_{\mathcal{E}} = \begin{bmatrix} x^{\mathcal{L}} & y^{\mathcal{L}} & z^{\mathcal{L}} \end{bmatrix}^T, \tag{A.20}$$

where $x^{\mathcal{L}}$, $y^{\mathcal{L}}$ and $z^{\mathcal{L}}$ are column vectors. This transformation is only valid for circular orbits.

Bibliography

[1] K. T. Alfriend, R. V. Srinivas, P. Gurfil, J. P. How, and L. S. Breger. *Spacecraft Formation Flying: Dynamics, control and navigation.* 2010.

[2] O. Bik, J. J. C. M.; Visser, P. N. A. M.; Jennrich. LISA satellite formation control, 2007.

[3] Rich Burns Chris Sabol and Craig A McLaughlin. Satellite Formation Flying Design and Evolution. *Journal of Spacecraft and Rockets*, 2001.

[4] David A. Vallado. *Fundamentals of Astrodynamics and Applications.* Fourth edi edition.

[5] ESA. https://earth.esa.int/web/guest/missions/3rd-party-missions/current-missions/grace.

[6] ESA. http://www.esa.int/Our_Activities/Operations/Cluster_II_operations.

[7] M. Morari F. Borrelli, A. Bemporad. *Predictive Control for linear and hybrid systems.* 2014.

[8] Gene F Franklin, J David Powell, and Abbas Emami-Naeini. *Feedback Control of Dynamic Systems*, volume 7. 2002.

[9] Pini Gurfil. *Modern Astrodynamics.* 2006.

[10] Bertil Westergren Lennart Rade. *Mathematics Handbook for Science and Engineering.* Fifth edit edition.

[11] Hyung-Chul Lim and Hyochoong Bang. Adaptive control for satellite formation flying under thrust misalignment. *Acta Astronautica*, 65(1-2), 2009.

[12] J. Löfberg. YALMIP : A Toolbox for Modeling and Optimization in MATLAB.

[13] Paul McNamara and Giuseppe Racca. Introduction to {LISA} Pathfinder. (LISA-LPF-RP-0002), 2009.

[14] NASA. http://www.nasa.gov/mission_pages/hubble/story/index.html.

[15] Per Johan Nicklasson Raymond Kristiansen. Spacecraft formation flying: A review and new results on state feedback control. *Acta Astronautica*, 2009.

[16] Raymond J. Sedwick Samuel Schweighart. High-Fidelity Linearized J2 Model for Satellite Formation Flight. *Journal of Guidance, Control and Dynamis*, 2002.

[17] Oliver Montenbruck Sunny Leung. Real-Time Navigation of Formation-Flying Spacecraft Using Global-Positioning-System Measurements. *Journal of Guidance, Control and Dynamis*, 2005.

[18] J. Jorgensen W. Xiang. Formation Flying: A Subject Being Fast Unfolding In Space, 2005.